DRL 126
DRD Se 8

DOE/JPL-955567-83/12
Distribution Category UC-63

TRIANNUAL REPORT

on the

DESIGN, ANALYSIS AND TEST VERIFICATION OF ADVANCED ENCAPSULATION SYSTEMS

For Period Ending

July 31, 1983

Contract 955567
6321-44

Prepared by:

Alexander Garcia III

Approved by:

Nick Mardesich
Manager, Advanced Programs

SPECTROLAB, INC.
12500 Gladstone Avenue
Sylmar, California 91342

November 1983

The JPL Flat-Plate Solar Array Project is sponsored by the U.S. Department of Energy and forms part of the Solar Photovoltaic Conversion Program to initiate a major effort toward the development of low-cost solar arrays. This work was performed for the Jet Propulsion Laboratory, California Institute of Technology by agreement between NASA and DOE.

TABLE OF CONTENTS

Section 1.0

SUMMARY

Final reports have been completed on the thermal, structural, and optical work done during Phase III. These documents are included in this report as Appendices A, B, and C. The final electrical report was included in the previously thirdly report (March, 1983). An additional polyurethane module was completed.

Section 2.0

INTRODUCTION

This program will develop the analytical methodology for advanced encapsulation designs. From these methods design sensitivities will be established for the development of photovoltaic module criteria and the definition of needed research tasks.

The program consists of four phases. In Phase I analytical models were developed to perform optical, thermal, electrical and structural analyses on candidate encapsulation systems. From these analyses several candidate encapsulation systems were selected for qualification testing during Phase II. Additionally, during Phase II, test specimens of various types will be constructed and tested to determine the validity of the analysis methodology developed in Phase I.

During Phase II the following items will be covered:

1. Correction of identified deficiencies and/or discrepancies between analytical models developed during Phase I and relevant test data obtained during Phase II of the above contract.

2. Improvement and extension of prediction capability of present analytical models.

3. Generation of encapsulation engineering generalities, principles, and design aids for photovoltaic module design.

From these items the sensitivity of module performance to various material properties will be determined. This study will enable the intelligent direction of research into assessment of module life potential by analyzing those materials and their properties which through aging would most influence module performance.

In Phase IV a final optimum design based on knowledge gained in Phases I, II and III will be developed and delivered to JPL.

Section 3.0

TECHNICAL DISCUSSION

3.1 FINAL REPORTS

Final reports have been completed on the thermal, structural, and optical work done during Phase III. These documents are included in this report as Appendices A, B, and C. The final electrical report was included in the previous thirdly report (March 1983).

3.2 MODULE CONSTRUCTION

To avoid problems with bubbles trapped beneath cells a second modification of the polyurethane casting process for assembly of the polyurethane layup was made. This procedure differs from the previous one in that the Craneglas is not put onto a flooded polyurethane surface. This eliminates bubbles trapped under the Craneglas which were previously a problem. The procedure follows:

1. The hardboard was prepared with wood ribs epoxied to the 1/8" 4' x 4' board.

2. Strips of 20 CP 3120 polyester film (3M) were glued to the back of the substrate using 4910 pressure sensitive adhesive (3M).

3. The top of the substrate was then spray painted with Krylon interior/exterior enamel 1502 (Borden). This is an alkyd based flat white paint.

4. Holes were made in the substrate for electrical termination.

5. The substrate was placed ribs down.

6. The surface was flooded with polyurethane.

7. A layer of .003" Craneglas was placed on the surface.

8. The primed cell circuit was then placed on a board, one end of the circuit lightly held, and the board slowly pulled away to allow the circuit to fall on the flooded surface.

9. Additional polyurethane was then pumped on the layup until the surface was completely covered.

10. Primed (Dow Corning Z6020 5% in methanol) Tedlar 100BG 3OUT was then rolled onto the layup to complete the module.

11. A weighted steel plate was placed on the module and the polyurethane allowed to cure.

This module was similar to the last one made. Only a very few bubbles marred its appearance. The problem was that bubbles became trapped under the cells and later during the curing worked their way to the surface. This is a difficult problem to solve in a manual process. It was decided by JPL personnel to discontinue work on polyurethane modules and continue work on the "creditcard" method.

Section 4.0

CONCLUSIONS AND RECOMMENDATIONS

There are no conclusions and recommendations for this period.

Section 5.0

PLANNED ACTIVITIES

During the next period Spectrolab will begin investigations into the feasibility of using transparent conductive materials as front surfaces of solar cells.

APPENDIX A

THERMAL ANALYSIS

James F. Coakley and James M. Kallis
Hughes Aircraft Company
El Segundo, California

June 1983

CONTENTS

LIST OF ILLUSTRATIONS

LIST OF TABLES

SUMMARY

The following thermal analysis tasks were performed in this phase of the encapsulation contract:

1. The solar cell temperatures predicted by the thermal model developed in the first part of the contract were compared with measured values. The agreement was very close (within 4 °C). The difference between the cell and air temperatures was found not to be proportional to the insolation over the entire range of parameters of interest, but the proportionality is a fairly good approximation for insolation values greater than approximately 60 mW/cm^2.
2. The sensitivity of the cell temperature to the wind speed and to the module thermal resistance was investigated.
3. Reduced-variable master curves and a procedure by which the cell temperature can be calculated by those not having access to a large computer program were developed. It is recommended that additional work be performed to 1) incorporate additional parameters into the dimensional groups, 2) develop a master curve or curves for the optical analysis, and 3) determine how simple the thermal/optical calculation can be made while retaining sufficient accuracy (that is, prediction of cell temperatures to within a few °C).

1.0 INTRODUCTION

1.1 BACKGROUND

Temperature is a key factor in the electrical efficiency of a solar cell, because the efficiency decreases monotonically with increasing cell temperature. For example, the efficiency of a single-crystal silicon cell decreases by approximately 0.005 for each °C increase in the cell temperature. Therefore thermal characteristics are important in the design of a photovoltaic module encapsulation system.

Accordingly thermal investigations have been performed throughout this encapsulation contract. In the first part of the contract, a method was developed for predicting cell temperatures and other thermal quantities, and various sensitivity studies were performed (Reference 1). In the second part of the contract, laboratory tests were performed to measure cell temperatures under controlled conditions, and the measured temperatures were compared with temperatures predicted by the aforementioned thermal model (Reference 2).

1.2 PRESENT INVESTIGATION

In this (the third) part of the contract, the earlier work was extended. The predictions were compared with several sets of test data; these comparisons are described in Section 2 of this report. The sensitivity studies were extended to parameters other than those investigated earlier; these calculations are described in Section 3. Reduced-variable master curves for the thermal analysis were developed; they are described in Section 4.

2.0 COMPARISON BETWEEN THERMAL MODEL AND TEST DATA

The cell temperatures predicted by the thermal model developed in the first part of the contract were compared with the temperatures measured in the following tests:

1. The Nominal Operating Cell Temperatures (NOCTs) measured by JPL for the Spectrolab Block II module.
2. The cell temperatures measured by Spectrolab and Hughes in the second part of this contract.

The NOCT is defined (Reference 3, p. A-1) as the cell temperature T_C measured in the Nominal Terrestrial Environment (NTE), which is specified as follows:

Insolation = 80 mW/cm^2

Air temperature T_A = 20 °C

Average wind speed = 1 m/s

Module mounting: tilted, open back, open circuit.

2.1 SPECTROLAB BLOCK II MODULE NOCT

The NOCT test data for the Spectrolab Block II (130 kW) module are reported in Reference 3. The tests were conducted in natural sunlight on 14 January 1977 with a tilt angle of 55 degrees. The sky was blue and clear, and the wind speed was between 2½ and 7 mph (1-3 m/s). Data were taken in the morning with the air temperature between 52 and 67 °F (11-19 °C) and in the afternoon with the air temperature between 61 and 68 °F (16-20 °C). The values of $T_C - T_A$ were lower in the afternoon than in the morning. The approximately half dozen measured values of the NOCT (insolation = 80 mW/cm^2) were 20-23 °C higher than the air temperature.

The predicted NOCT, calculated assuming an AM 1.5 spectrum at normal incidence, was 24 °C higher than the air temperature.

Thus, the predicted value

$$T_C - T_A = 24\ ^\circ C \text{ (predicted)}$$

agrees closely with the measured values

$$T_C - T_A = 20\text{-}23\ ^\circ C \text{ (measured)}.$$

As an additional comparison between the thermal model and the test data, the model was employed to predict the relation between $T_C - T_A$ and the insolation S. JPL has reported (for example, in Reference 4) that $T_C - T_A$ is proportional to S (at least, for S > 40 mW/cm^2) and is largely independent of the air temperature. The predicted relation between $T_C - T_A$ and S for the Spectrolab Block II modules is shown in Figure 2-1. The curve was calculated for normal incidence with a fixed tilt angle (34 °), an open circuit, and a constant air temperature (20 °C). Thus everything was held fixed except the insolation. There appears to be no test performed in this manner with which this prediction can be compared. The predicted curve approaches a straight line passing through the origin at high insolation

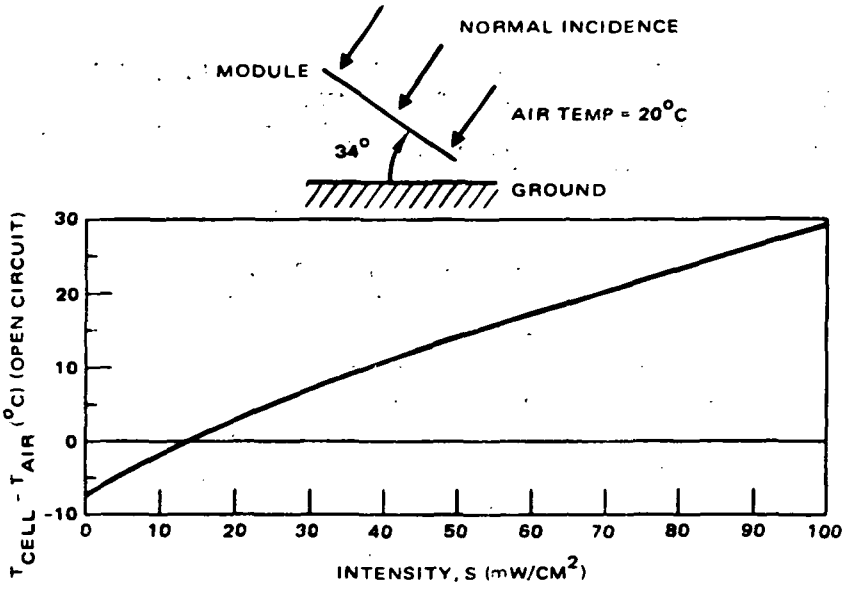

Figure 2-1. Predicted dependence of open-circuit cell temperature on intensity for Spectrolab Block II module.

values (above 60 mW/cm^2). At lower insolation values, however, the curve becomes significantly nonlinear and $T_C - T_A \rightarrow -7$ °C as $S \rightarrow 0$. In other words, at nighttime, the cell becomes cooler than the air and approaches a temperature between the air temperature and the sky temperature (the sky temperature is −5 °C, 25 °C lower than the air temperature).

2.2 SPECTROLAB/HUGHES ENCAPSULATION CONTRACT TESTS

In contrast to the outdoor, relatively uncontrolled NOCT measurements discussed above, the tests performed in the second part of this contract were performed in a laboratory under controlled conditions. The thermal model was employed to predict the cell temperatures for the test conditions, and the predicted and measured cell temperatures are presented in Reference 2.

Examination of the data indicates that only a few of the measurements are comparable with the model. These are the measurements for the center cell in the module. (The others are not comparable, either because the center-cell thermocouple was of questionable validity or because only the edge-cell temperature was measured.) These measurements are compared with the predictions in Table 2-1. The agreement is excellent. For the tests in which the module had a high backside emissivity, as will actual production modules, the predicted and measured cell temperatures agreed

TABLE 2-1. COMPARISON BETWEEN PREDICTED AND MEASURED TEMPERATURES OF CENTER CELL FOR SPECTROLAB/HUGHES ENCAPSULATION CONTRACT TESTS

Module	Test Run No.	Back-side Emis-sivity	Temperature (°C)				% Error $\frac{T_{CP} - T_A}{T_{CM} - T_A} - 1$ (%)	
			Air T_A	Cell				
				Meas-ured T_{CM}	Predic-ted T_{CP}	Differ-ence $T_{CP} - T_{CM}$		
TM-1	5	0.95	39.6	80.1	80.2	0.1	0.2	High module backside emissivity
↓	8	↓	39.9	69.1	69.4	0.3	1.0	
TM-3	1	0.9	40.6	74.5	75.8	1.3	3.8	
↓	4	↓	40.2	84.3	88.0	3.7	8.4	
TM-1	1	0.04	41.6	72.1	78.5	6.4	21.0	Low module backside emissivity
↓	4	↓	41.6	85.1	93.0	7.9	18.2	
TM-3	5	0.03	38.7	84.2	92.7	8.5	18.7	
↓	8	↓	40.7	74.6	79.4	4.8	14.2	

to within 4 °C. For the tests in which the module had a low backside emissivity, the agreement was within 9 °C, which is not as close but still is good. The larger difference for the low emissivity probably was caused by the surface having a higher emissivity than expected. It is difficult to maintain surfaces at a low emissivity, and a small increase in the emissivity is a large percentage increase. This would cause the prediction to overestimate the cell temperature by a larger amount for the low emissivity than for the high emissivity, which is exactly what happened.

3.0 SENSITIVITY STUDIES

In the first part of the contract, the sensitivity of the cell temperature to the pottant thickness, pottant thermal conductivity, front (sun) side emissivity, and back (shade) side emissivity were investigated.

In this third part of the contract, the sensitivity to the wind speed and the thermal resistances to cell-to-frontside and cell-to-backside conduction were studied. The computer code developed in the first part of the contract, which is described in Reference 1, was used for these calculations.

The results are shown in Figures 3-1 through 3-7. Figures 3-1 through 3-3 show the sensitivity of the cell temperature to the cell-to-frontside and cell-to-backside conductive thermal resistances for wind speeds of 0, 25, and 50 ft/sec, respectively. Figures 3-4 through 3-7 show the sensitivity to the wind speed and the cell-to-backside conductive thermal resistance for values of the cell-to-frontside conductive thermal resistance of 1, 10, 100, and 1000 cm^2-°C/W, respectively.

4.0 DEVELOPMENT OF REDUCED-VARIABLE MASTER CURVES

The objective of this analysis was to enable a module designer, not having access to the computer program with which the predictions described in Sections 2 and 3 above were made, to estimate the sensitivity of the cell temperature to various parameters. The approach was to derive reduced-variable master curves from the equations that govern the relevant thermal phenomena.

(Text continued on page 13)

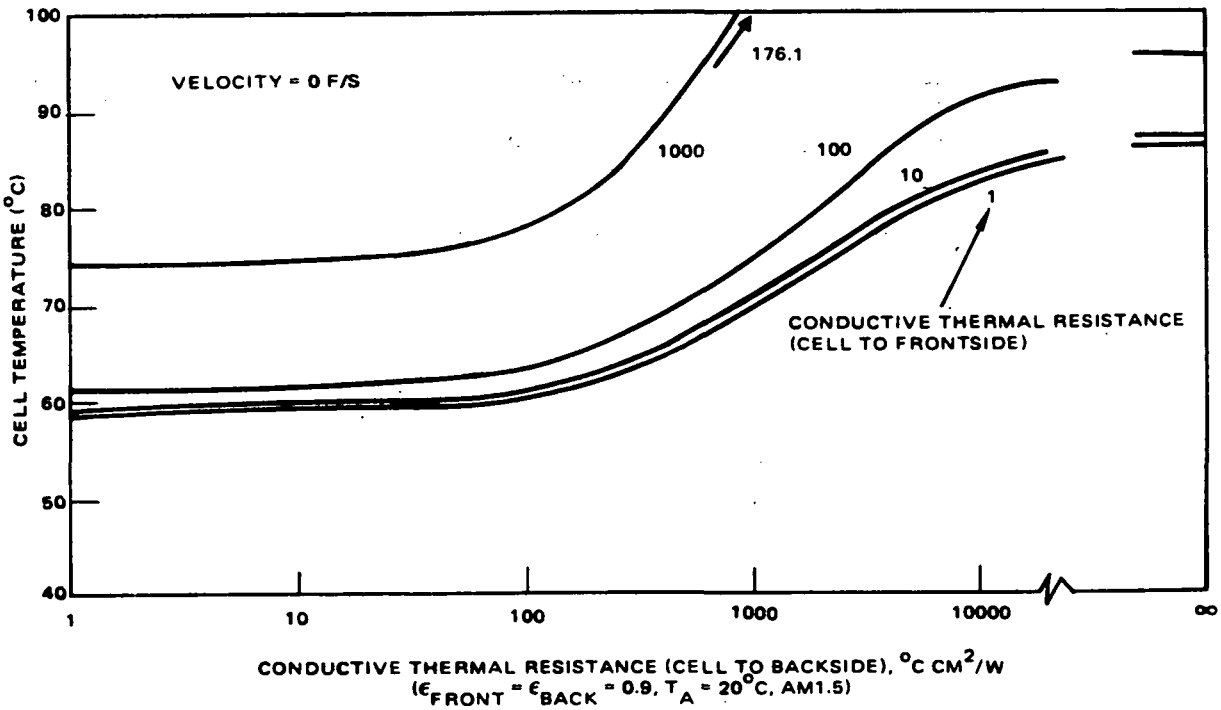

Figure 3-1. Cell temperature versus thermal resistance, wind speed = 0 f/s.

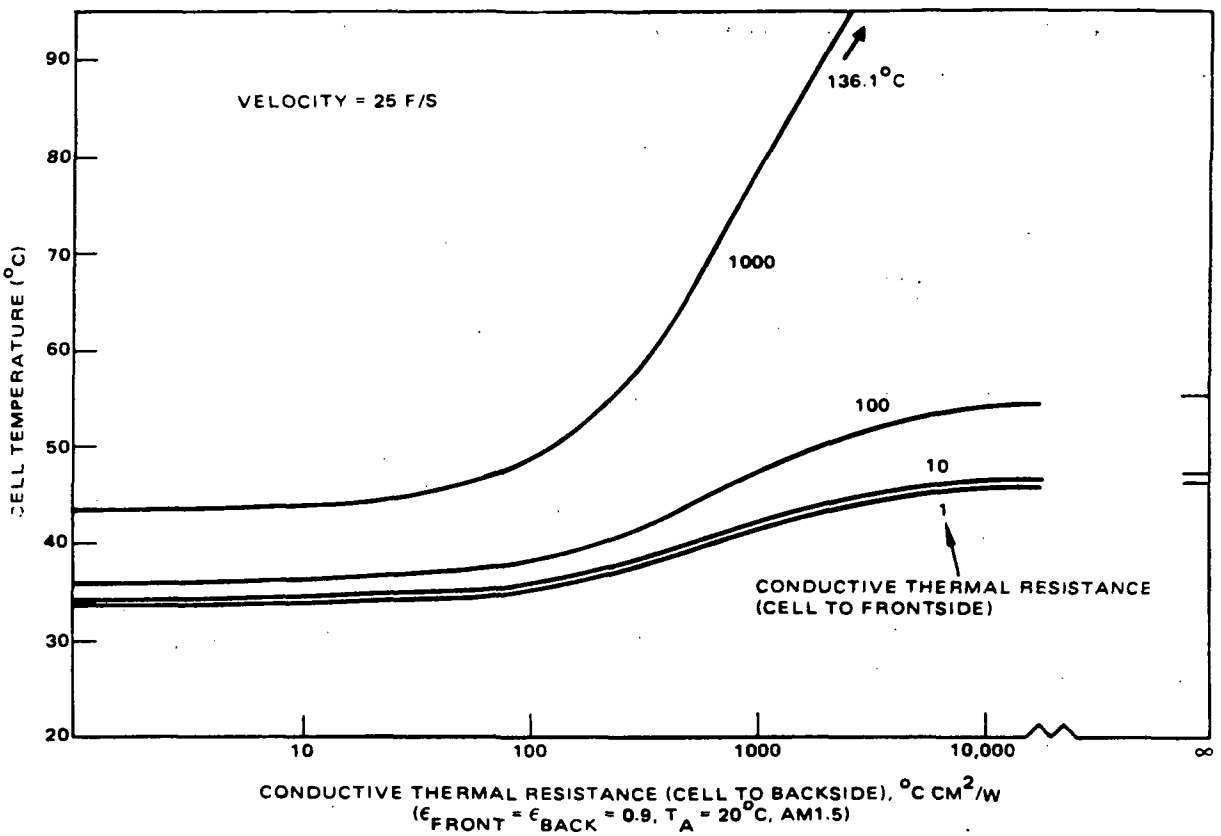

Figure 3-2. Cell temperature versus thermal resistance, wind speed = 25 f/s.

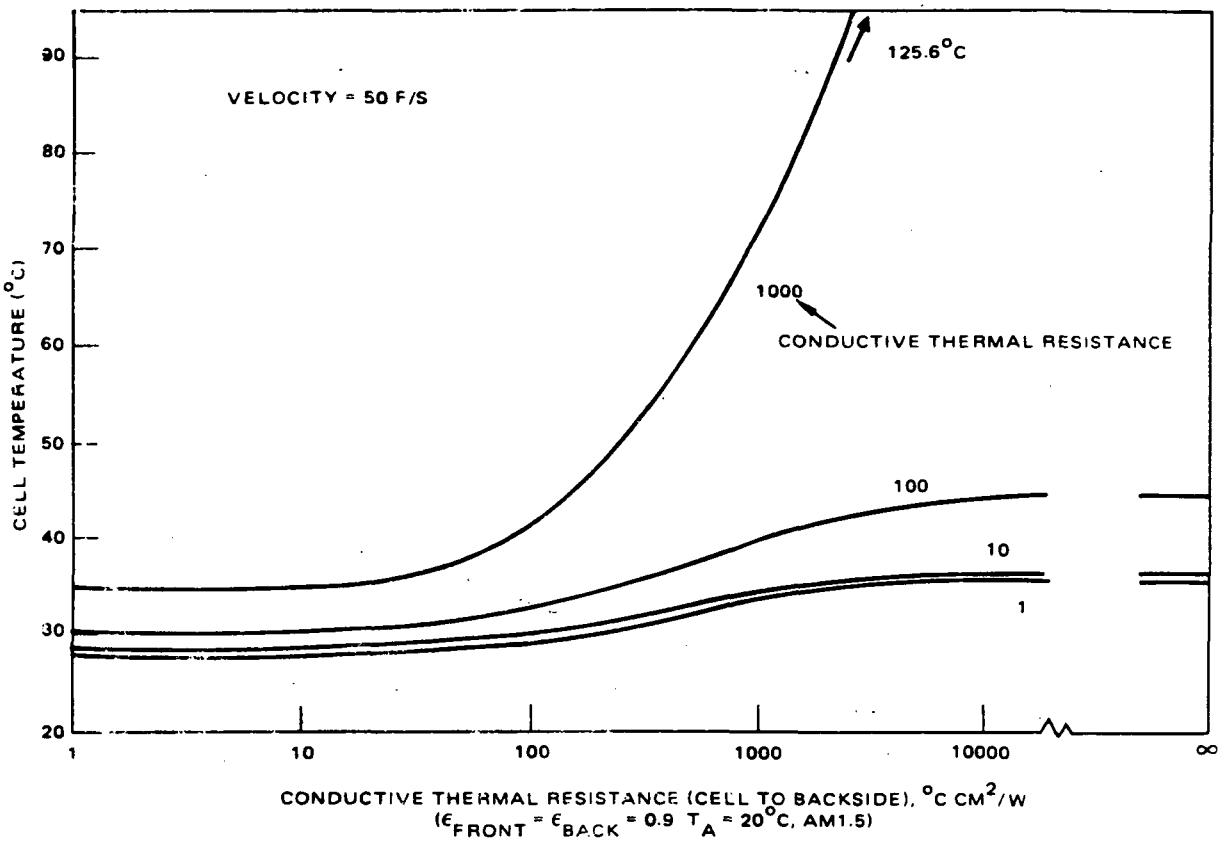

Figure 3-3. Cell temperature versus thermal resistance, wind speed = 50 f/s.

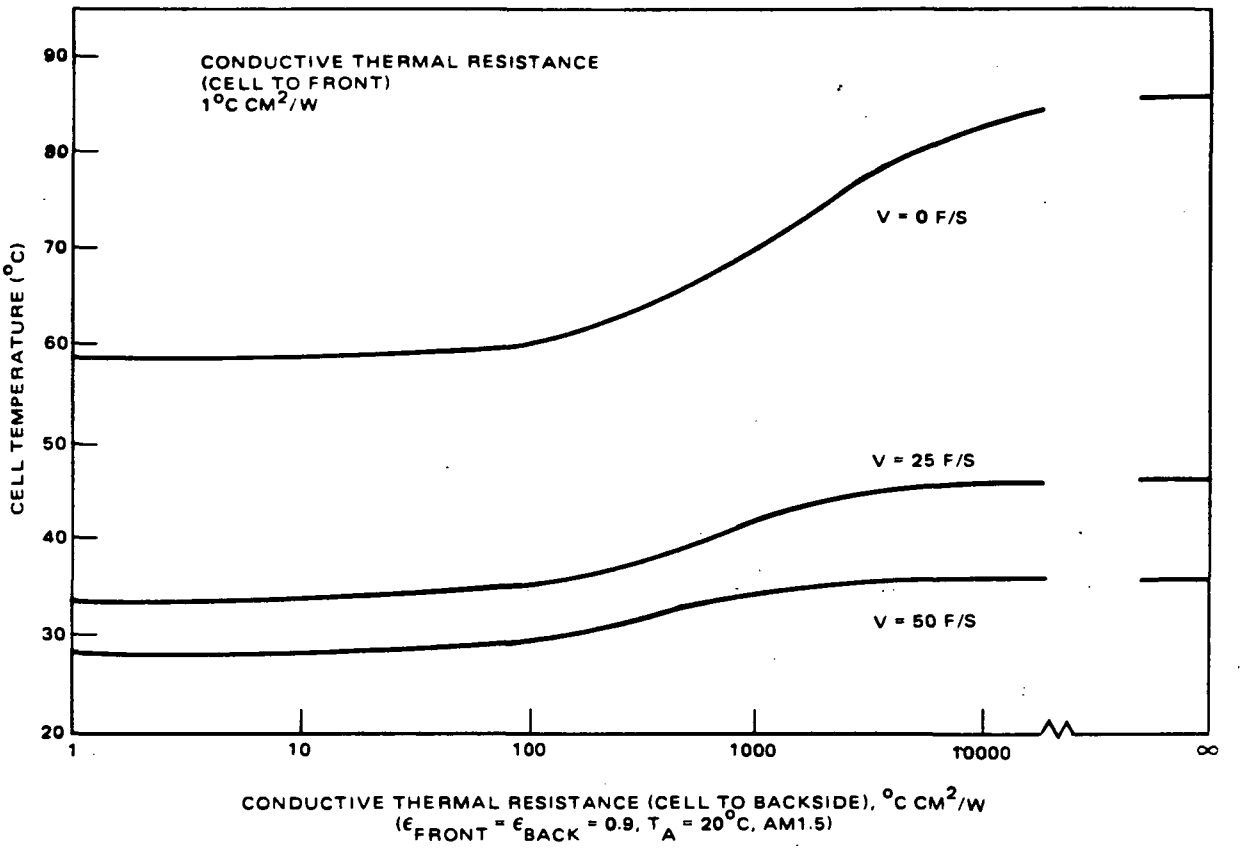

Figure 3-4. Cell temperature versus thermal resistance, $R_F = 1^oC\ cm^2/w$.

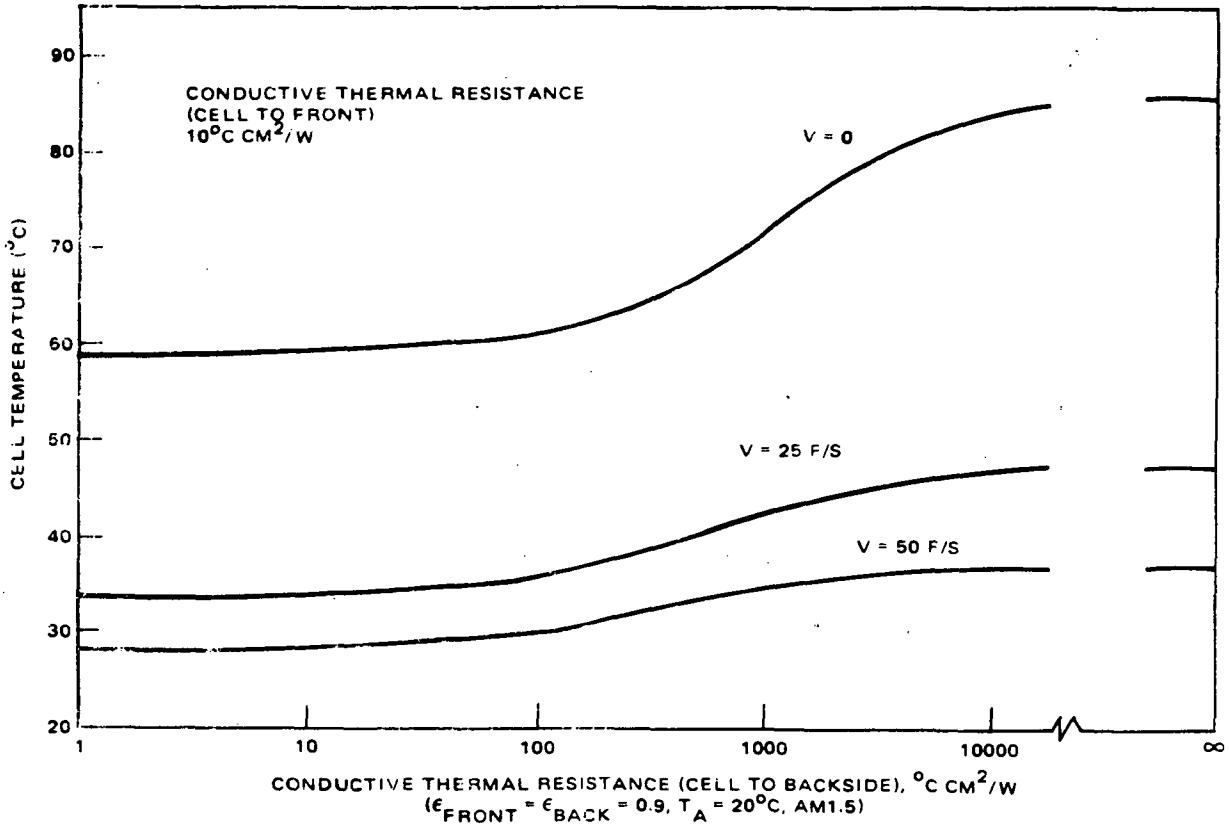

Figure 3-5. Cell temperature versus thermal resistance, $R_F = 10^oC\ cm^2/w$.

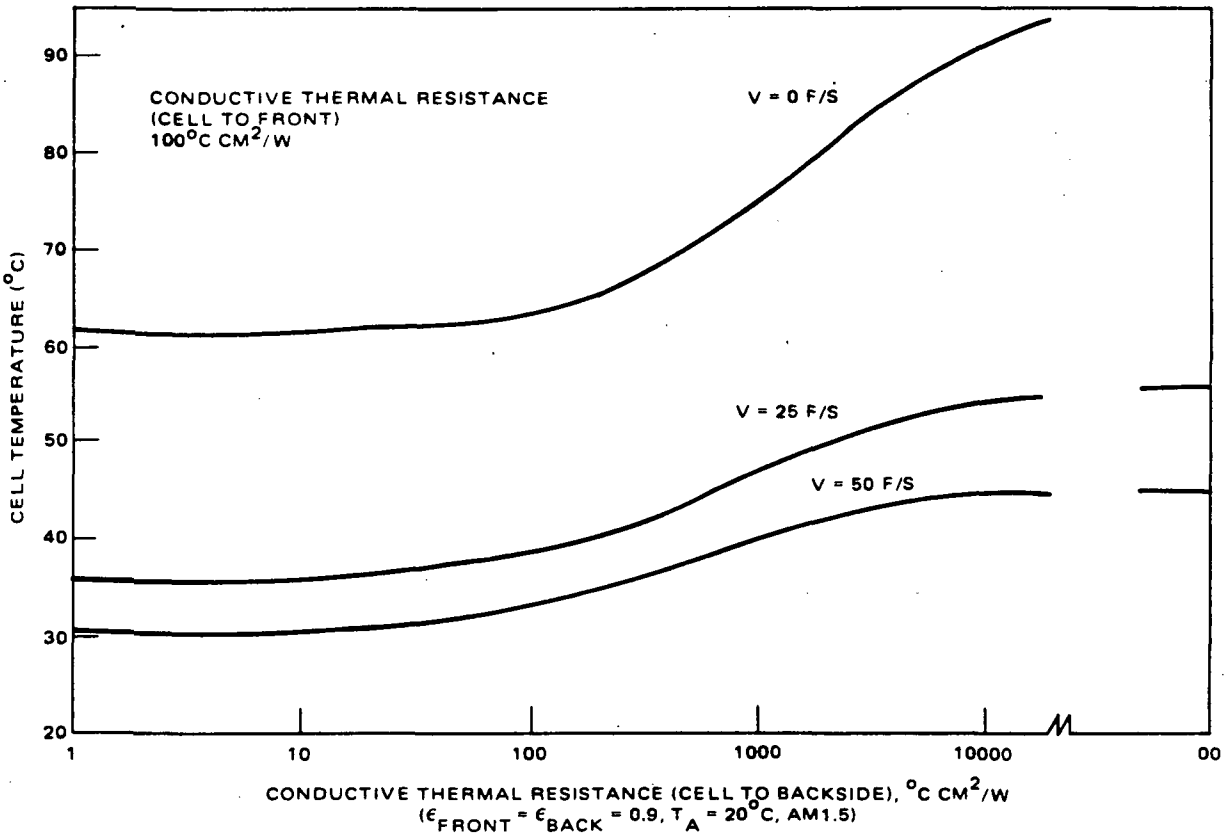

Figure 3-6. Cell temperature versus thermal resistance, $R_F = 100^{\circ}C\ cm^2/w$.

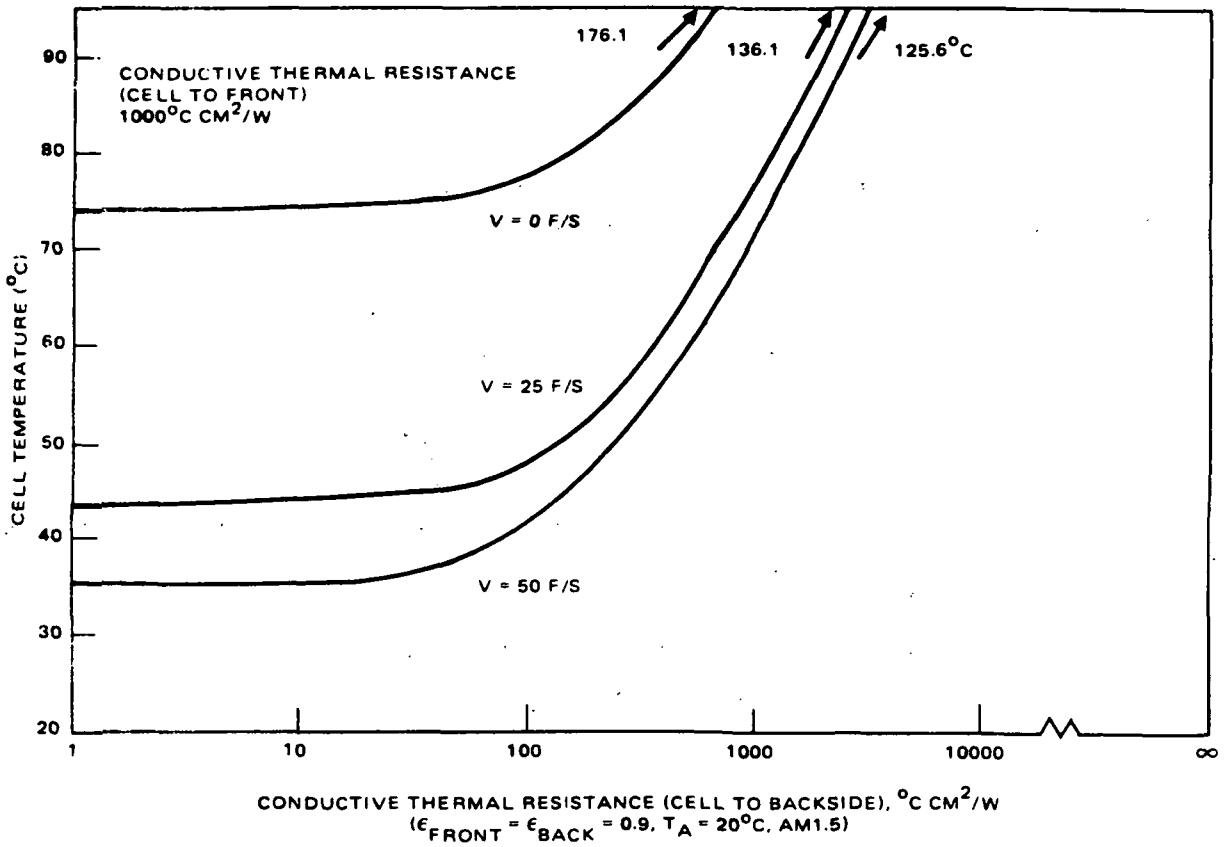

Figure 3-7. Cell temperature versus thermal resistance, R_F = 1000°C cm²/w.

4.1 DERIVATION OF EQUATIONS

4.1.1 Separation of Optical and Thermal Calculations

The first step in the development was to recognize that the optical and thermal calculations are independent of each other.

The optical calculation consists of evaluating the effects of 1) the reflections at interfaces between materials having different refractive indices and 2) the absorption in these materials. The output of the optical analysis is the power per unit area absorbed in the module—the desired absorption by the cell and the undesired absorption elsewhere. In the temperature range of interest here, the reflectances and absorptances are independent of the material temperatures. Also, absorption and reradiation in the encapsulant are neglected. Therefore the optical calculation can be performed prior to the thermal calculation, and calculated absorptions can be used as inputs to the thermal analysis.

In the derivation described herein, the absorbed power density was taken to be a given quantity. It can be calculated by the computer program described in Reference 1. The development of reduced-variable master curves to perform the optical analysis was not undertaken.

4.1.2 Simplification of the Thermal Model

The second step was to simplify the thermal model.

The detailed model described in Reference 1 is shown in Figure 4-1. It accounts for the absorption Q_C by the cell, as well as the absorptions in the front cover (Q_1) and pottant (Q_2) and the intercell spacing (Q_1', Q_2', and Q_C'). Conduction within the module is modelled by 14 nodes.

The simplified model is shown in Figure 4-2. The absorptions other than by the cell have been neglected, that is,

$$Q_1 = Q_2 = Q_1' = Q_2' = Q_C' = 0. \qquad (4\text{-}1)$$

Conduction within the module was modelled by only 3 nodes (cell, front (sun-side) surface, and back (shade-side) surface), rather than 14. The simplified model is a good approximation, because previous calculations with the detailed model have shown that the power absorbed in the module is absorbed primarily in the cell. Ignoring the intercell spacing is equivalent to assuming that the module packing factor is 100 percent.

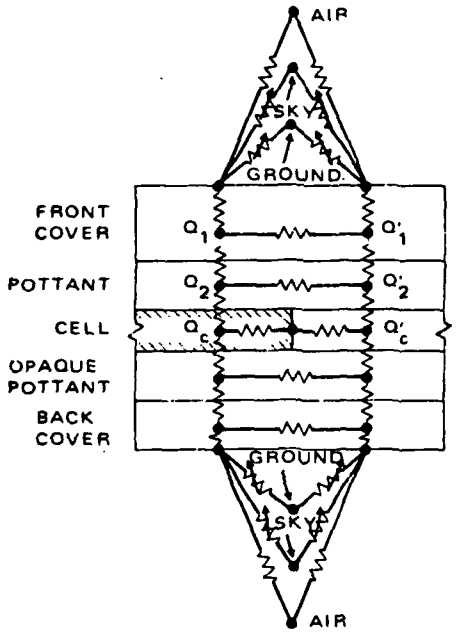

Figure 4-1. Detailed model developed in first part of contract.

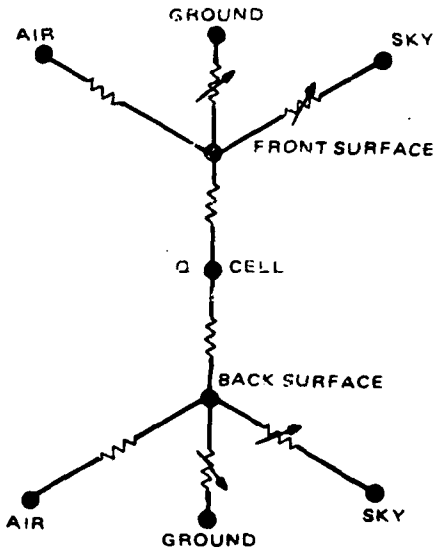

Figure 4-2. Simplified model employed to develop master curves.

4.1.3 Solution of Simplified Thermal Model

Writing energy balances for each of the three module nodes resulted in three equations in three unknowns. Combining these equations and manipulating terms yielded the following implicit equation for the cell temperature:

$$G_{eq}^{T} T_C - Q = E, \tag{4-2}$$

where

$$E = \left(\frac{G_{CD}}{G_{CD} + G_{eq}} (T_A G_{CV} + T_S G_{RS} + T_G G_{RG})\right)_F + \left(\frac{G_{CD}}{G_{CD} + G_{eq}} (T_A G_{CV} + T_S G_{RS} + T_G G_{RG})\right)_B, \tag{4-3}$$

Q = power per unit area absorbed by the cell,

T_C = cell temperature,

T_A = air temperature,

T_S = sky temperature,

T_G = ground temperature,

G = unit thermal conductance,

and F and B refer to the front and back, respectively, of the module. In this formula, the unit thermal conductances are as follows:

G_{CD} = module unit thermal conductance

$$= 1/\left(\Sigma (t/k)\right) \tag{4-4}$$

(where k = thermal conductivity of each layer of the module, t = thickness of that layer, and the summation is taken over all the layers between the cell and the surface),

G_{CV} = unit thermal conductance for convection from the surface to the air

$$= a\left[(T_M - T_A)\cos\psi\right]^{1/3} + bV \tag{4-5}$$

(where a and b are constants, T_M = module surface temperature, ψ = module tilt angle relative to the ground, and V = wind speed),

G_{RS} = unit thermal conductance for radiation from the surface to the sky

$$= \sigma \epsilon F_S (T_M + T_S)(T_M^2 + T_S^2) \tag{4-6}$$

(where σ = Stefan-Boltzmann constant, ϵ = module surface emissivity, and F_S = view factor between the module surface and the sky),

G_{RG} = unit thermal conductance for radiation from the surface to the ground

$$= \sigma \epsilon F_G (T_M + T_G)(T_M^2 + T_G^2) \qquad (4\text{-}7)$$

(where F_G = view factor between the module surface and the ground),

$$G_{eq} = G_{CV} + G_{RS} + G_{RG}, \qquad (4\text{-}8)$$

and

$$G_{eq}^T = G_{CD}^F + G_{CD}^B - \left(\frac{G_{CD}^2}{G_{CD} + G_{eq}}\right)^F - \left(\frac{G_{CD}^2}{G_{CD} + G_{eq}}\right)^B. \qquad (4\text{-}9)$$

(In Equation (4-9), T, F, and B are superscripts, whereas 2 is an exponent.) The unknown cell temperature T_C appears explicitly on the left-hand side of Equation (4-2), but it also appears implicitly in the equations for the unit thermal conductances for convection and radiation.

Equation (4-2) can be solved for the cell temperature to yield

$$\boxed{T_C = \frac{Q + E}{G_{eq}^T}} \qquad (4\text{-}10)$$

In this equation, E and G_{eq}^T depend on T_C, whereas Q does not. Once Q is calculated by an optical analysis, T_C can be evaluated by graphical or iterative methods. An iterative method is described below.

4.2 ITERATIVE METHOD FOR CALCULATING CELL TEMPERATURE

The method consists of the following steps:

1. Make an initial estimate of the cell temperature.
2. Enter the estimated cell temperature into graphs of the dimensional groups appearing in Equations (4-2) and (4-3), including the aforementioned unit thermal conductances for radiation and convection, as functions of the cell temperature.
3. Enter these estimated conductances into a nomograph to obtain a new estimate of the cell temperature.

4. Repeat steps (2) and (3) until the cell temperature estimates have converged to the desired accuracy.

To perform steps (2) and (3), the designer would have to have access to a set of graphs appropriate to the parameters of his/her module design. Sets of graphs appropriate to a wide range of parameters have not yet been prepared. However, to illustrate the use of the method, one such set of graphs has been prepared and is presented in the example described below.

4.3 EXAMPLE

The following typical parameters were selected:

Module tilt angle $\psi = 34\,^{\circ}$.

Wind speed $V = 1$ m/s.

Air temperature $T_A = 20\,^{\circ}C$.

Ground temperature $T_G = 20\,^{\circ}C$.

Sky temperature $T_S = -5\,^{\circ}C$.

Module front surface emissivity $\epsilon_F = 0.9$.

Module back surface emissivity $\epsilon_B = 0.9$.

Insolation $S = 97$ mW/cm^2 (AM 1.5).

Power per unit area absorbed by the cell $Q = 78$ mW/cm^2 (80 percent of the insolation).

Module front unit thermal conductance

$$G_{CD}^{F} = 1 \text{ W/(cm}^2\text{-}^{\circ}\text{C)}.$$

Module back unit thermal conductance

$$G_{CD}^{B} = 1 \text{ W/(cm}^2\text{-}^{\circ}\text{C)}.$$

For this example, the initial estimate T_{C_1} of the cell temperature was obtained from the following empirical formula (Reference 4):

$$T_{C_1} = T_A + m\,S, \tag{4-11}$$

where

$$m = 0.3\ ^{\circ}\text{C-cm}^2\text{/mW}. \tag{4-12}$$

(As shown herein in Section 2, Equation (4-11) is an oversimplified formula for the cell temperature. However, it is adequate for obtaining an initial estimate.) For the parameters of this example, the result is

$$T_{C_1} = 49\,^{\circ}C.$$

For the parameters of this example, the unit thermal conductances are plotted versus the cell temperature for various wind speeds in Figures 4-3 and 4-4. In each graph, the initial estimate T_{C_1} of the cell temperature has been entered for a wind speed of 1 m/s to obtain the corresponding value of the dimensional group.

A nomograph by which the cell temperature can be evaluated for the values of these dimensional groups and of the absorbed power density Q is shown in Figure 4-5. For the parameters of this example, the nomograph is entered as shown in the figure to obtain the second estimate T_{C_2} of the cell temperature:

$$T_{C_2} = 50\,^{\circ}C.$$

Thus the second estimate of the cell temperature is 1 °C higher than the first estimate. This iterative process can be continued until the cell temperature converges to the desired accuracy.

5.0 CONCLUSIONS

1. The cell temperatures predicted by the thermal model developed in the first part of the contract agree to within 4 °C with measured temperatures.
2. The difference between the cell and air temperatures is not proportional to the insolation over the entire range of parameters of interest. This proportionality is, however, a fairly good approximation for insolation values higher than approximately 60 mW/cm^2.
3. Reduced-variable master curves and a procedure by which the cell temperature can be calculated without a large computer program have been developed.

6.0 RECOMMENDATIONS

1. The thermal master curves should be extended to:
   - Investigate whether the dependences on wind speed and module tilt angle can be incorporated into the dimensional groups
   - Add insolation values lower than 70 mW/cm^2 to the nomograph

(Text continued on page 21)

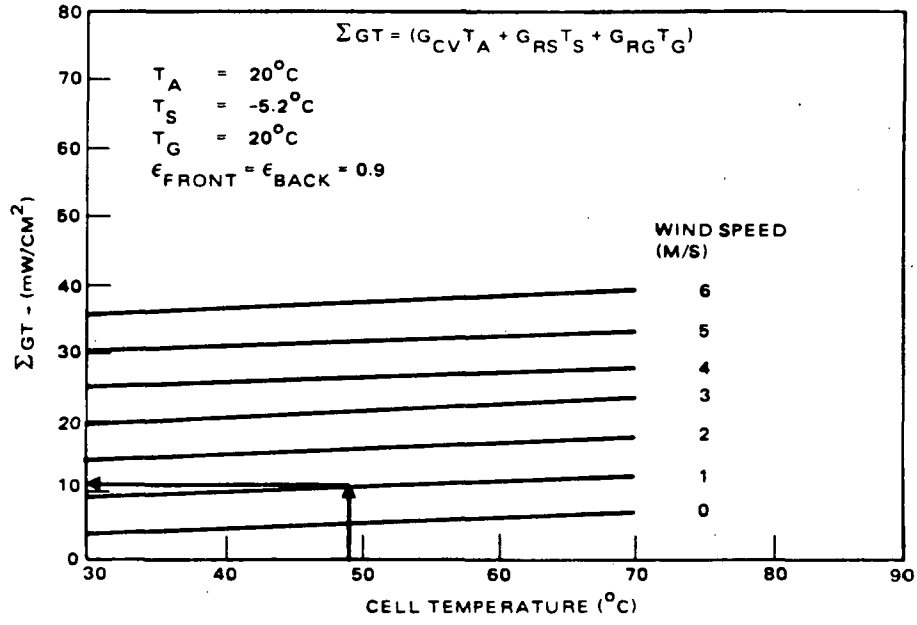

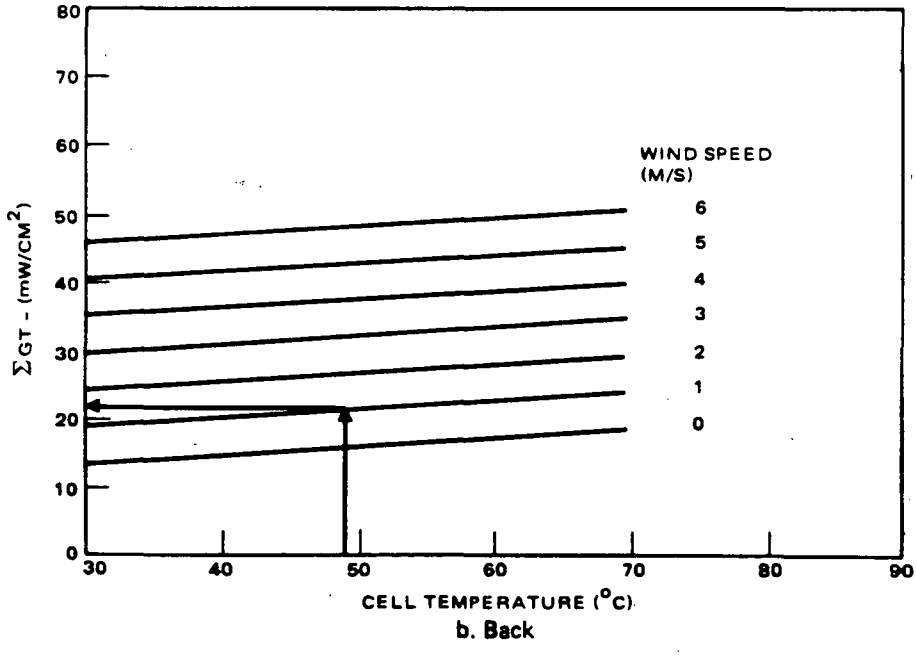

Figure 4-3. Dimensional group – ΣGT versus cell temperature.

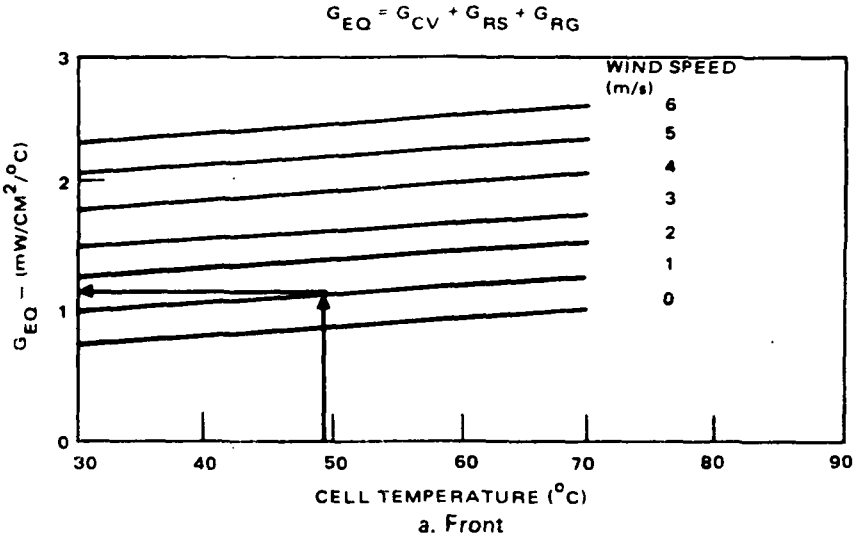

a. Front

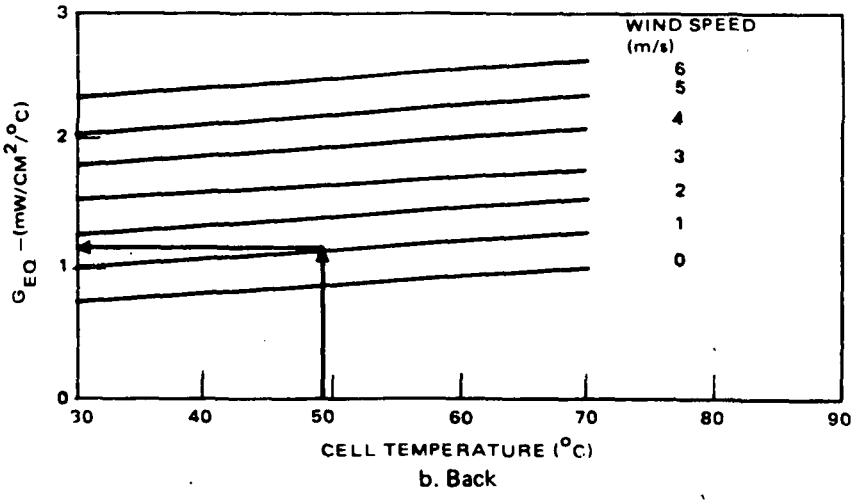

b. Back

Figure 4-4. Dimensional group – G_{eq} versus cell temperature.

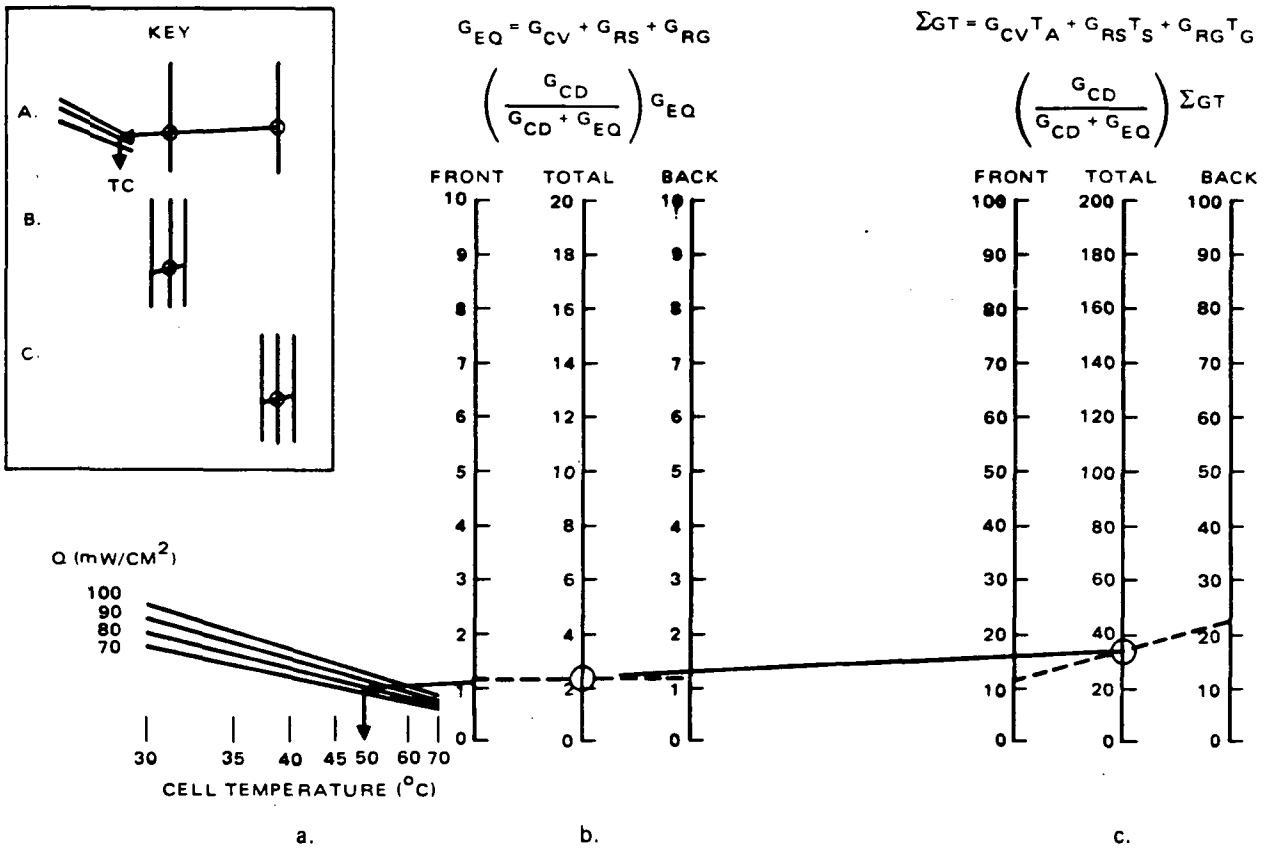

Figure 4-5. Cell temperature as function of Q, G_{CD} and dimensional groups G_{eq}, ΣGT.

- Investigate whether a single reference temperature can be used in place of the three sink temperatures (air, ground, and sky) presently used.

2. An optical master curve or curves should be developed so that the power per unit area absorbed by the cell can be calculated by those not having access to a large computer program.
3. An investigation should be undertaken to determine how simple the thermal/optical calculation procedure can be made while retaining sufficient accuracy (that is, prediction of NOCT to within a few °C).

ACKNOWLEDGEMENTS

Technical discussions with C. D. Coulbert, E. F. Cuddihy, A. Garcia, and I. R. Jones were very helpful for the work described herein.

REFERENCES

1) A. Garcia and C. P. Minning, "Design, Analysis, and Test Verification of Advanced Encapsulation Systems, Interim Report for Period Ending 1 October 1980," DOE/JPL-95567-81/4, November 1981.

2) "Analysis and Test Verification of Encapsulation Systems for Terrestrial Photovoltaic Modules," Hughes Aircraft Company Report No. FR 81-70-1091, October 1981.

3) J. W. Stultz and L. C. Wen, "Thermal Performance Testing and Analysis of Photovoltaic Modules in Natural Sunlight," JPL Report 5101-31, 29 July 1977.

4) L. Wen, "An Investigation of the Effect of Wind Cooling on Photovoltaic Arrays," JPL Report 5101-201, March 1982.

APPENDIX B

STRUCTURAL ANALYSIS

L.B. Duncan
Hughes Aircraft Company
El Segundo, California

June 1983

CONTENTS

LIST OF ILLUSTRATIONS

SUMMARY

In the first phase of the encapsulation contract, analytical models were developed to predict solar cell stress in flat-plate, terrestrial, photovoltaic modules subjected to out-of-plane deflection and temperature excursions (Reference 1). These analytical models were used to predict solar cell stress for modules having glass, wood, or steel structural panels, pottant thicknesses from 1 to 20 mils, and 10 mil thick silicon solar cells. In the second phase of the contract, tests were performed to verify the analytical models (Reference 2).

After the completion of phase one, E. F. Cuddihy of JPL developed a reduced-variable master curve from the computer predictions of solar cell thermal stress (Reference 3). The master curve generalized the computer results and provided a desktop capability for predicting solar cell stress for any combination of pottants and structural panels. However, the master curve was only valid for 4 $\times$ 4 in, 10 mil thick silicon solar cells, on which the analytical predictions were based.

In the current phase of the program, a second reduced-variable master curve was developed from the computer predictions for out-of-plane deflection of a module. In addition, both master curves were generalized to include important solar cell parameters. This work completes the requirements of Revision-D of the Statement of Work.

The master curves are useful design tools for predicting solar cell stress for any combination of structural panel, pottant, and solar cell. They are applicable for square, rectangular, or round cells. However, these curves have not been validated for "thin-film" solar cells so they should not be used for solar cells which have a thickness less than 2 mils.

The master curves do not depend upon the geometry of the structural panel. However, the pressure stress master curve does require the maximum stress in the structural panel. This stress must be determined by separate analysis techniques, available in the literature, which take into account the support conditions, geometry, and magnitude of the pressure load.

The master curves indicate the following trends:

1. Cell stress decreases as the pottant thickness is increased or the pottant elastic modulus is decreased.

2. Cell stress decreases as the elastic modulus of the cell decreases. Cell stress increases as the cell size increases. Cell stress also increases as the cell thickness decreases.

3. Thermal stress in a cell is a function of the difference between the coefficients of thermal expansion of the cell and the structural panel.

It is recommended that the structural models be extended to accommodate "thin-film" solar cells. The cell thickness parameter range should be extended to cells thinner than 1 mil. In addition, the cell length parameter range should be extended to a cell length of 12 inches.

1.0 INTRODUCTION

1.1 BACKGROUND

Mechanical loading such as wind and snow pressure, acceleration due to earthquakes, and imposed twist due to support settlement or misalignment generates stress in a terrestrial photovoltaic module. As the module deflects under load, strain in the structural panel transfers through the pottant to the solar cell. Similarly, when the module undergoes changes in temperature, differential thermal expansion between the structural panel and the cell generates stress in the cell.

In the first phase of the contract, analytical models were developed to predict stress in the solar cells due to out-of-plane deflection and thermal loading. The analyses focused on 4 ×4 ft. simply-supported modules which consisted of glass, steel, or wood structural panels, 4 ×4 in., 10 mil thick silicon solar cells, and pottants of various thicknesses and elastic moduli. The results of the computer analyses, which are contained in the Phase-One Summary Report (Reference 1), consisted of families of curves for each of the structural panel materials.

In the second phase of the contract, thermal and deflection tests were performed to verify the analytical models. The deflection tests produced interesting results and provided a rationale for improving the analytical model. Unfortunately, the thermal tests were inconclusive due to equipment calibration problems. However, the thermal stress model has predicted the high incidence of cell breakage experienced in both aluminum and hardboard panel modules (Reference 3).

After the completion of phase one, E.F. Cuddihy of JPL developed a reduced-variable master curve from the analytical predictions of solar cell thermal stress (Reference 3). The master curve provided for any combination of structural panel and pottant. However, the master curve was valid only for 4 ×4 in., 10 mil thick silicon solar cells on which the analytical predictions were based.

1.2 PRESENT INVESTIGATIONS

In the current phase of the contract, a second master curve was developed for the prediction of solar cell stress for out-of-plane deflection

of a module. In addition, the analytical models and master curves were extended to include the following solar cell parameters:

- Elastic Modulus
- Thickness
- Coefficient of Thermal Expansion
- Size
- Geometry: square, rectangular, or round.

These additions complete the requirements of Revision-D of the Statement of Work.

1.3 OVERVIEW

The following sections summarize the structural analysis activity. Section 2 explains the physical behavior of modules under load and the computer approach which was employed to predict solar cell stress. Section 3 presents the master curves and discusses the sensitivity of cell stress to the parameters of the reduced-variables. A sample problem is presented in Section 4 to demonstrate the use of the master curves. Finally, recommendations for further work are given in Section 5.

2.0 METHOD

This section describes the physical behavior of a terrestrial photovoltaic module subjected to pressure and thermal loading and the analytical models which were developed to predict the resultant solar cell stress.

In the first phase of the contract, the analytical models were used to predict cell stress for modules having glass, steel, or wood structural panels, pottants of various thickness and elastic moduli, and 10 mil thick, 4 $\times$ 4 in. silicon solar cells. The results of these analyses were reported in the Phase-One Summary Report (Reference 1). In the current phase of the contract, additional analyses were performed to determine the change in cell stress for changes in cell parameters such as Young's modulus, thickness, and cell size.

The results of these analyses were used to develop the master curves for pressure and thermal loading, which are described in Section 3.0.

2.1 PRESSURE-DEFLECTION LOADING

2.1.1 Physical Behavior

Terrestrial photovoltaic modules subjected to wind pressure deflect under the load. As the module deflects, the strain in the structural panel transfers through the pottant, generating stress in the solar cells. The cell stress is highly dependent upon the pottant stiffness.

If the pottant is stiff (i.e., has a high modulus of elasticity), the structural panel and cell act together as a rigid beam. Plane sections remain plane and cell stress is a function of the distance from the neutral axis of the cross-section.

If the pottant is elastomeric, the cell is permitted to move relative to the structural panel. The relative movement reduces the cell stress.

Since cell stress is caused by the deflection and curvatures of the structural panel, it is important to understand the behavior of the structural panel as it deforms. When module deflections are less than one-half of the structural panel thickness, the linear, small deflection plate bending theory applies. However, cost-effective module design dictates the use of the thinnest material that can withstand the environmental loads, so module deflections can be several times larger than the thickness of the structural panel.

When module deflection exceeds one-half the thickness of the structural panel, the panel stretches like the head of a drum. This stretching causes membrane tension stresses in the central area of the panel. Since simply-supported modules are typically free to move inplane, the membrane tension stresses are equilibrated by membrane compressive stresses along the edges of the panel, as illustrated in Figure 2-1. These membrane stresses are not accounted for by the linear, small-deflection theory of structural mechanics (Reference 4). In order to accurately predict the stresses and deflection, non-linear, large-deflection theory must be used.

Unfortunately, it is not practical, in general, to solve a non-linear, large deflection problem without the aid of non-linear finite element computer analysis techniques. However, non-linear computer analysis techniques can be costly and time-consuming. Since it was necessary to analyze a large number of module configurations, a cost-effective analysis approach was needed to evaluate the non-linear effects.

2.1.2 Analytical Model

It was recognized that the linear, small deflection theory could be used to analyze local cell-pottant-structural panel behavior once the local boundary conditions were derived using the non-linear, large deflection theory. Therefore, a linear, two-dimensional finite element model simulating the local cell-pottant-structural panel construction was developed for use in the parameter sensitivity studies. The MSC/NASTRAN structural analysis program was used.

The model consisted of rectangular plate elements which simulated the load-bearing layer, the pottant, the cell, and other layers such as front or back covers. As shown in Figure 2-2, only one half of a cell was modelled. Symmetric boundary conditions were imposed along the plane through the cut edge of the cell, and free-edge conditions were imposed along the plane between adjacent cells. In other words, the model behaves as a cantilever beam with the left-hand edge considered fixed and non-rotating.

Linear analyses were performed on this model to assess the effects of large module deflection induced membrane and bending stresses on local cell-pottant-structural panel behavior. This was accomplished by subjecting the module to two separate loading conditions. First, the free end of the structural panel was displaced in the axial (inplane) direction, which simulated membrane stretching. Second, a lateral displacement of the structural panel was imposed at the free end, which simulated bending.

The resultant strains in the load-bearing layer and the cell, as well as the ratio of these strains, were then determined. The strain ratio was assumed to remain invariant with deflection of the load-bearing layer. On the other hand, the strain ratio was assumed to be a function of pottant, cell, and load-bering layer parameters. Given a stress in the load-bearing layer, the cell stress could be determined by multiplying the load-bearing layer stress by the appropriate strain ratio.

The analysis model revealed the following:

1. Cell stress is highly dependent upon curvature (bending) of the load-bearing layer. However, cell stress is much less sensitive to membrane stretching. Therefore, the non-linear membrane stresses could be neglected. Cell stress predictions could be based upon the curvature of the structural panel.
2. Load-bearing layer stress is not influenced by the cell. This was shown by comparison with simple beam-bending calculations.

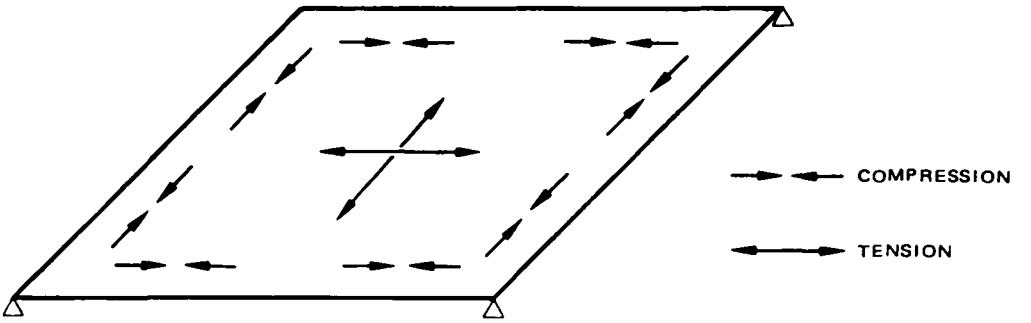

Figure 2-1. Membrane stresses in a simply-supported plate due to large deflection.

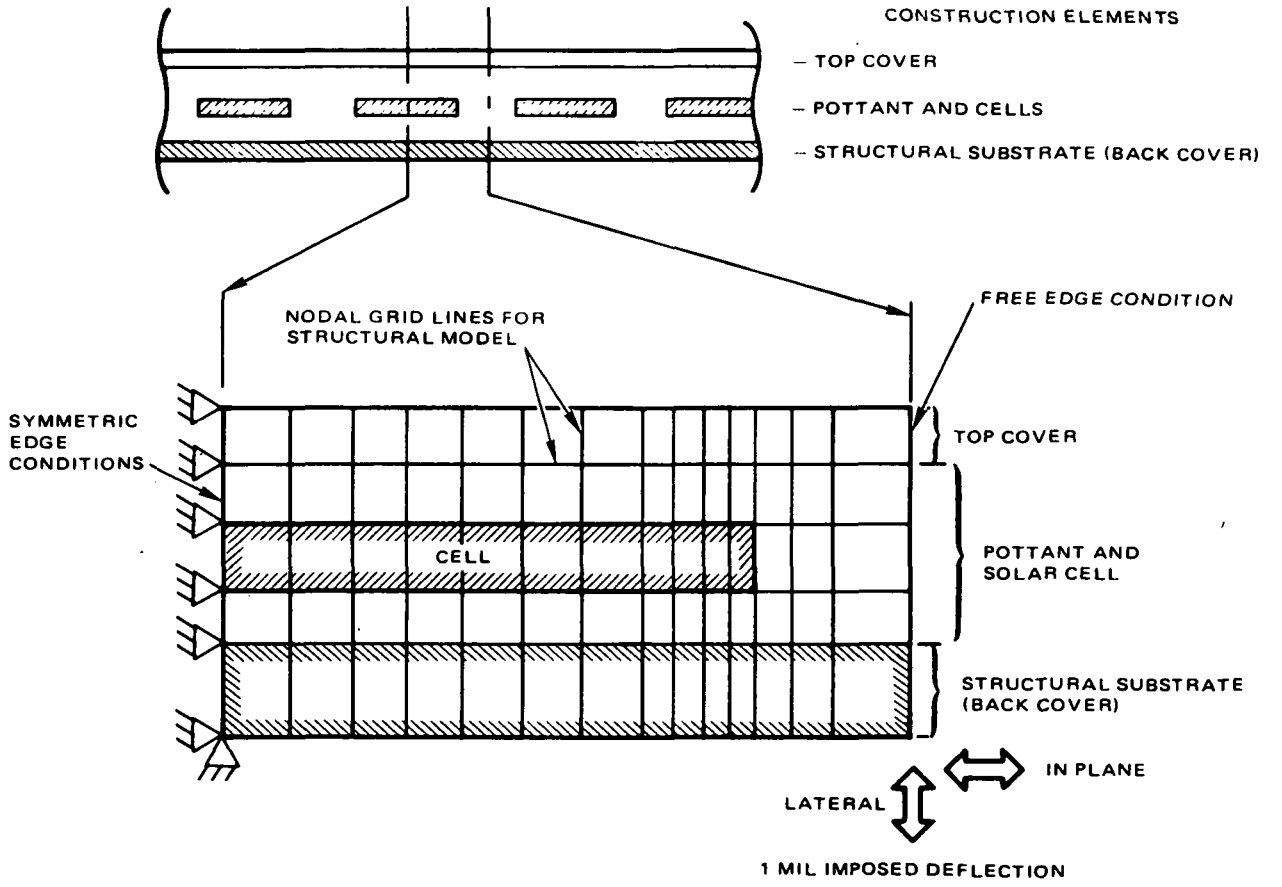

Figure 2-2. Finite-element structural model for determination of stresses in module construction elements in vicinity of a centrally-located cell.

3. The stress in a cell on the load side of a module consists of non-uniform compression. The stress in a cell on the anit-load side of a module is non-uniform tension, which consists of a membrane component and a bending component, as illustrated in Figure 2-3. The membrane component is due to the offset of the cell from the load-bearing layer. The bending component is due to the curvature of the cell.

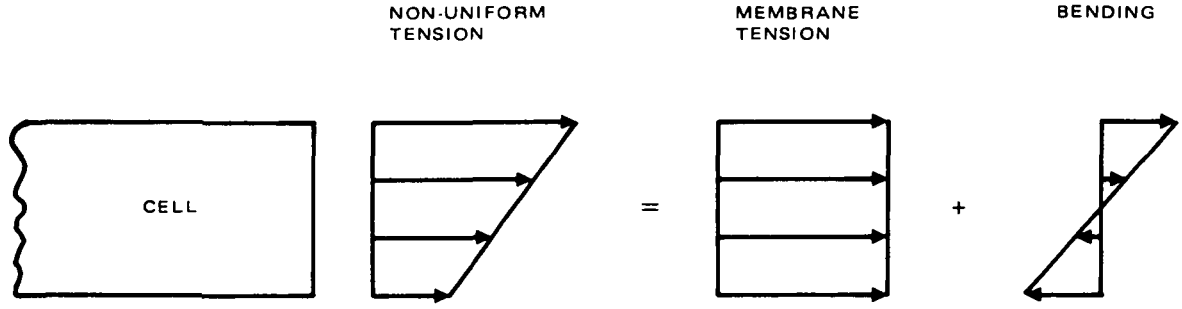

Figure 2-3. Components of stress in a solar cell on the anti-load side of a module.

2.1.3 Deflection Tests and Verification of the Model

The deflection tests, which were performed during the second phase of the contract, revealed the following:

1. The most highly stressed cells in a module are located at the corners of the structural panel, which are the locations of highest stress in the structural panel.
2. Cell stress predictions were accurate for 10 PSF module loading. For greater loads, the cell stress predictions had to be adjusted to account for the large deflection induced membrane stress in the structural panel. The membrane stress did not change the cell stress; however, it changed the previously described strain ratio. The adjustment for module loading is described in Section 3.

2.2 THERMAL LOADING

2.2.1 Physical Behavior

When a module undergoes a change in temperature, the solar cell and the structural panel expand (or contract) according to their respective coefficients of thermal expansion. If the coefficients of thermal expansion are different, the cell and the structural panel will not change length by the same amounts. If the resultant difference in lengths is not fully accommodated by the pottant, stress will be generated in the cell.

An elastomeric pottant will permit relative movement between the cell and the structural panel, thereby reducing the stress in the cell.

2.2.2 Analytical Model

The thermal stress analyses used the same two-dimensional NASTRAN model described in Section 2.1.2. In addition, a 5-1/2 cell, two-dimensional model, shown in Figure 2-4, was developed to determine variations in cell stress due to cell location in the module.

The 5-1/2 cell model revealed that the cell stress at the edge of the module was approximately 10 percent higher than the cell stress at the center of the module. Therefore, in the subsequent sensitivity analyses free-edge conditions were imposed at the boundary of the one-half cell model.

The boundary conditions imposed on the model permitted the cell and the load-bearing layer to interact as a function of their respective thermal stiffnesses, $E\alpha$, where E is the modulus of elasticity and α is the coefficient of thermal expansion. The interaction resulted in bending and stretching of the cross-section, as shown in Figure 2-5. In the figure, shear deformation of the elastomeric pottant is clearly shown.

For all cases studied, it was assumed that the module was isothermal and experienced a 100 °C temperature excursion from ambient. Temperature-invariant material properties (evaluated at 25 °C) were used in the studies. However, it is recognized that the pottant modulus increases with decreasing temperature. But the intent of the analysis was to predict trends, and since temperature-dependent material properties necessitate a non-linear analysis, the assumption of temperature-invariant properties was deemed acceptable.

2.2.3 Thermal Tests and Verification of the Model

The results of the thermal tests were inconclusive due to measurement system calibration problems and uncertainties in the material properties. However, the thermal stress model was used to predict the high incidence of cell breakage in both aluminum and hardboard panel modules (Reference 3). The model showed that large stresses in the silicon solar cells occur in aluminum modules because the thermal expansion coefficient of aluminum is relatively large. Cell fracture in experimental EVA-hardboard modules was shown to be partly due to the high hygroscopic expansion

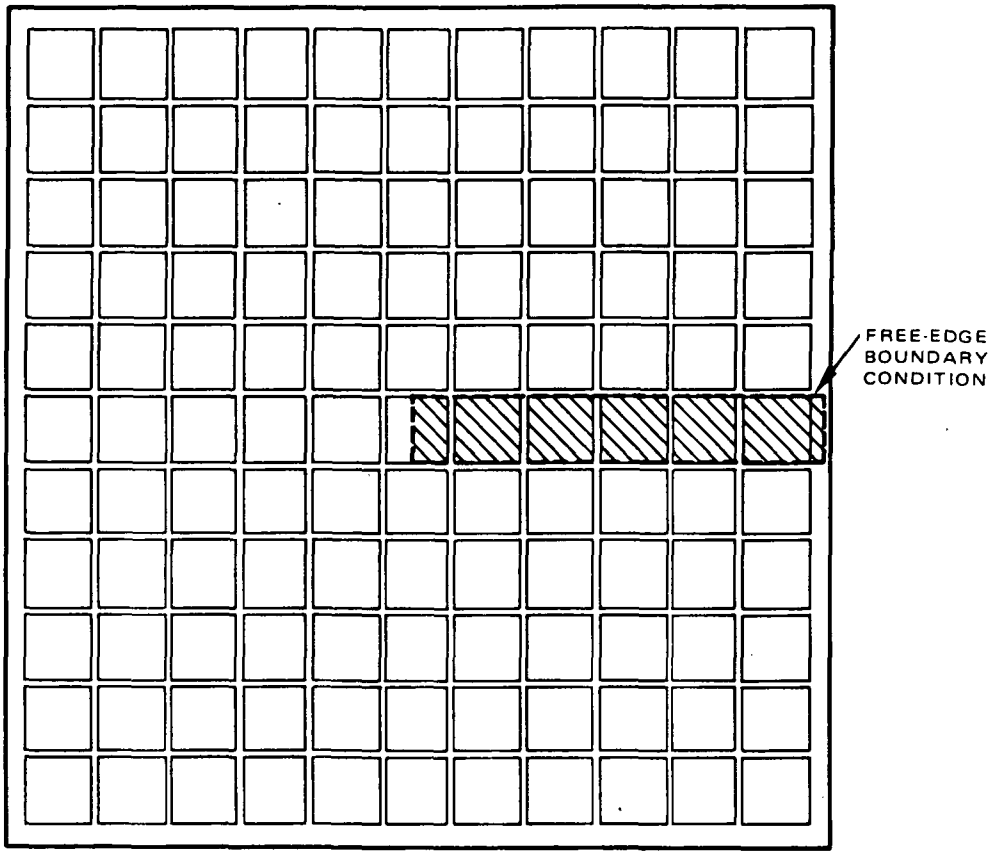

Figure 2-4. Structural model for determination of cell stress as a function of location in module.

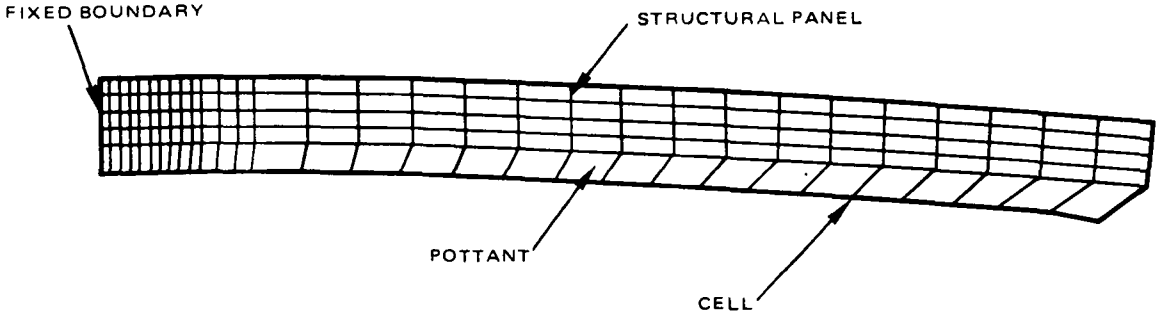

Figure 2-5. Deflection of structural panel pottant and cell for 100°C temperature excursion.

rate of the hardboard. On the basis of these predictions, therefore, the thermal stress model can be considered a useful design tool.

3.0 MASTER CURVES

3.1 Reduced-Variable Parameters

The master curves were developed by trial-and-error positioning of the analysis variables until the predictions for different module configurations merged into a composite curve for pressure loading and a composite curve for thermal loading. The development was aided by an awareness of physically meaningful variable groupings such as plate flexural stiffness (Et^3) and thermal stiffness ($E\alpha$). The reduced variables of the master curves contain those parameters which were found to significantly affect solar cell stress. Intercell spacing was not included because adjacent cells act independently. Although intercell spacing is an important interconnect design parameter, interconnect design considerations are not within the scope of this work.

The master curves are applicable for square, rectangular, or round solar cells. In addition, the master curves do not depend upon the geometry or support conditions of the structural panel.

3.1.1 Pressure Stress Master Curve

The master curve for pressure stress analysis is shown in Figure 3-1. The relationship between solar cell stress and the parameter variables was found to be

$$S_{CP} = \frac{S_{SP}\, E_C^{1/2}\, L_C^{1.15}}{E_{SP}\, t_{SP}\, t_P^{1/8}\, t_C^{1/3}}\, F_N\, (t/E)_P\, (1/Et^3)_{SP} \qquad (1)$$

where

S_{CP} = SOLAR CELL MAX PRESSURE STRESS
S_{SP} = STRUCTURAL PANEL MAX STRESS
E_{SP} = MODULUS OF STRUCTURAL PANEL
t_{SP} = THICKNESS OF STRUCTURAL PANEL
t_P = THICKNESS OF POTTANT
E_P = MODULUS OF POTTANT
E_C = MODULUS OF SOLAR CELL
t_C = THICKNESS OF SOLAR CELL
L_C = LENGTH OF SOLAR CELL

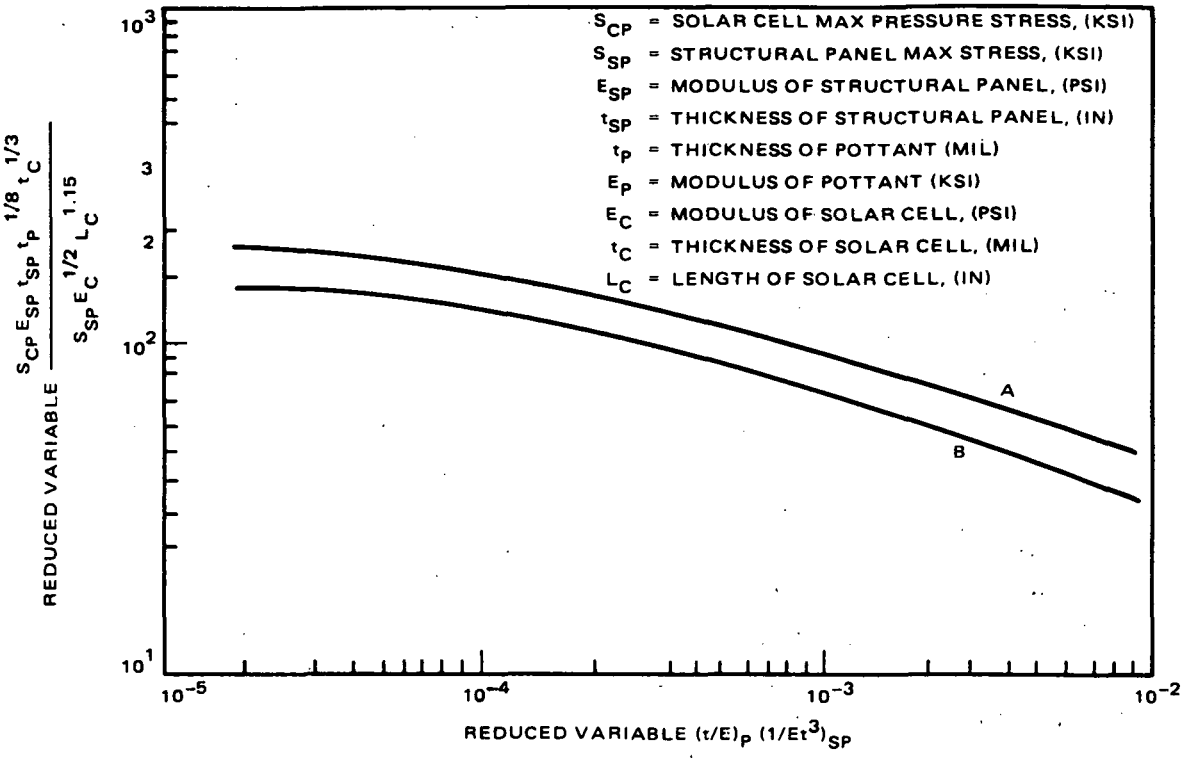

NOTE: USE CURVE A FOR PRESSURE ≤ 10 PSF USE CURVE B FOR PRESSURE = 50 PSF
FOR INTERMEDIATE LOADS, INTERPOLATE LINEARLY BETWEEN A AND B

Figure 3-1. Master curve for pressure stress analysis.

As seen in Figure 3-1, the cell stress decreases as the quantity $(t/E)_p(1/Et^3)_{SP}$ increases.

The key pottant parameters are Young's modulus E_p and thickness t_p. Cell stress decreases as the pottant stiffness decreases. For an elastomeric pottant, the stiffness decreases when the thickness is increased or Young's modulus is decreased. If the pottant is not elastomeric (i.e., $E_p > 10$KSI), cell stress does not decrease as the pottant thickness is increased. A stiff pottant does not permit relative movement between the cell and the structural panel. Therefore, consistent with conventional beam theory, cell stress for stiff pottants increases as the distance between the cell and the structural panel increases.

The important cell parameters are Young's modulus E_C, cell thickness t_C, and cell length L_C. Cell stress is proportional to $E_C^{1/2}$ and thus decreases as Young's modulus is decreased. Cell stress is proportional to $t_C^{-1/3}$ and thus is also decreased as the thickness is increased, perhaps because the cell is more resistant to strain as the thickness increases.

Cell stress is proportional to $L_C^{1.15}$ and thus decreases as the edge length decreases. As the length gets smaller, the cell deforms less as the module deflects. It should be noted that the edge length is defined as the longest edge for rectangular or square cells and the diameter for round cells.

The important structural panel parameters are Young's modulus E_{SP}, thickness t_{SP}, maximum panel stress S_{SP}, and the magnitude of the pressure load. Important parameter combinations are flexural stiffness, $(Et^3)_{SP}$, and membrane stiffness, $(Et)_{SP}$; the cell stress decreases as the panel stiffness increases.

The structural panel stress, S_{SP}, must be determined by separate analysis. For example, the design curve of Reference 5, shown in Figure 3-2, can be used to determine the maximum stress in a simply-supported plate subjected to uniform pressure loading. For a given pressure load, the panel stress decreases as the flexural stiffness $(Et^3)_{SP}$ increases. The cell stress is proportional to the panel stress.

The master curve consists of two curves which account for the magnitude of the pressure load. As shown in Figure 3-1, curve A is used when the module pressure load is less than or equal to 10 PSF. Curve B applies for a module load of 50 PSF, which represents a wind velocity of 100 MPH. For intermediate loading, interpolate linearly between Curves A and B.

3.1.2 Thermal Stress Master Curve

The master curve for thermal stress analysis is shown in Figure 3-3. The relationship between solar cell stress and the parameter variables is

$$S_{C:T} = \frac{\alpha_{SP} E_{SP}^{1/3} \Delta T E_C^{1/2} L_C^{1.5}}{t_C^{1/2}} \left(\frac{\alpha_{SP} - \alpha_C}{\alpha_{SP} - \alpha_S}\right) F_N \left((t/E)_P (E\alpha)_{SP}\right) \quad (2)$$

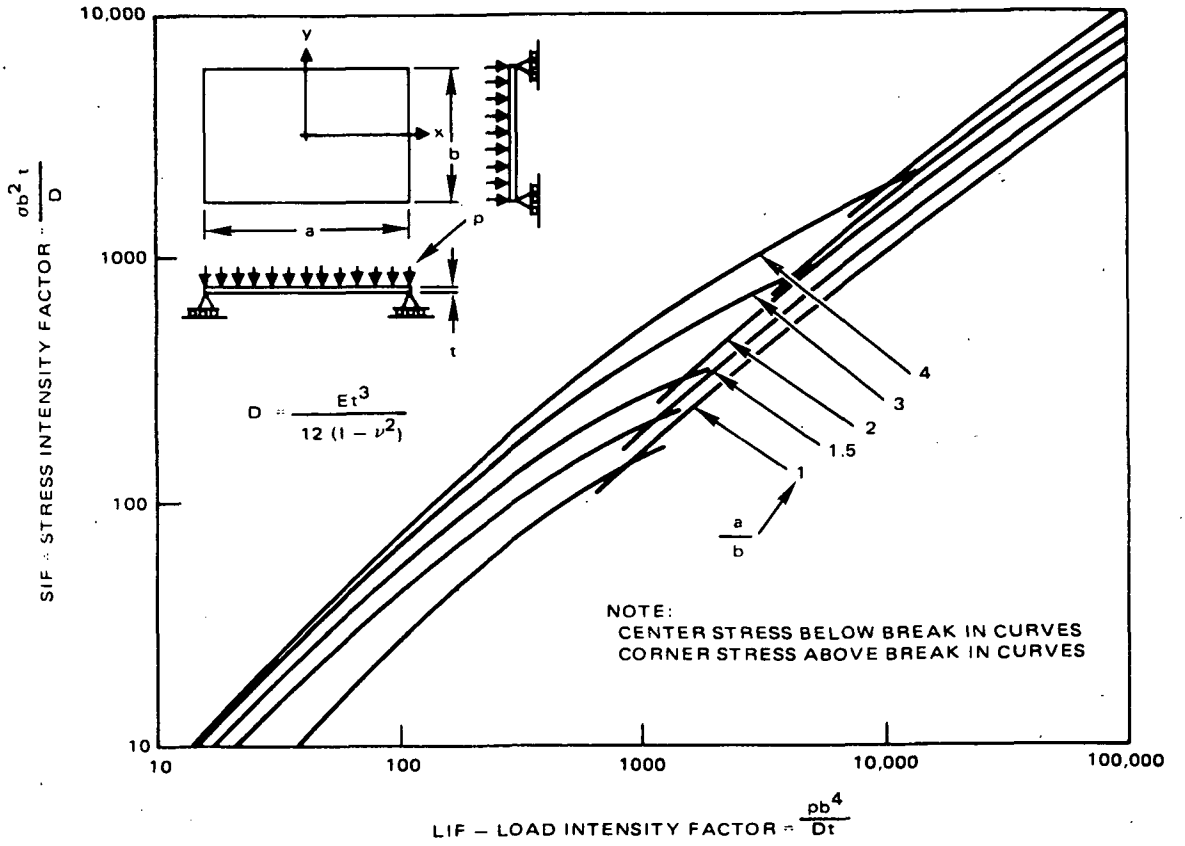

Figure 3-2. Stress intensity factor (SIF) versus load intensity factor (LIF) showing composite curves of the larger of the maximum positive stresses on plate (center bottom or top surface near corner) (Reference 5).

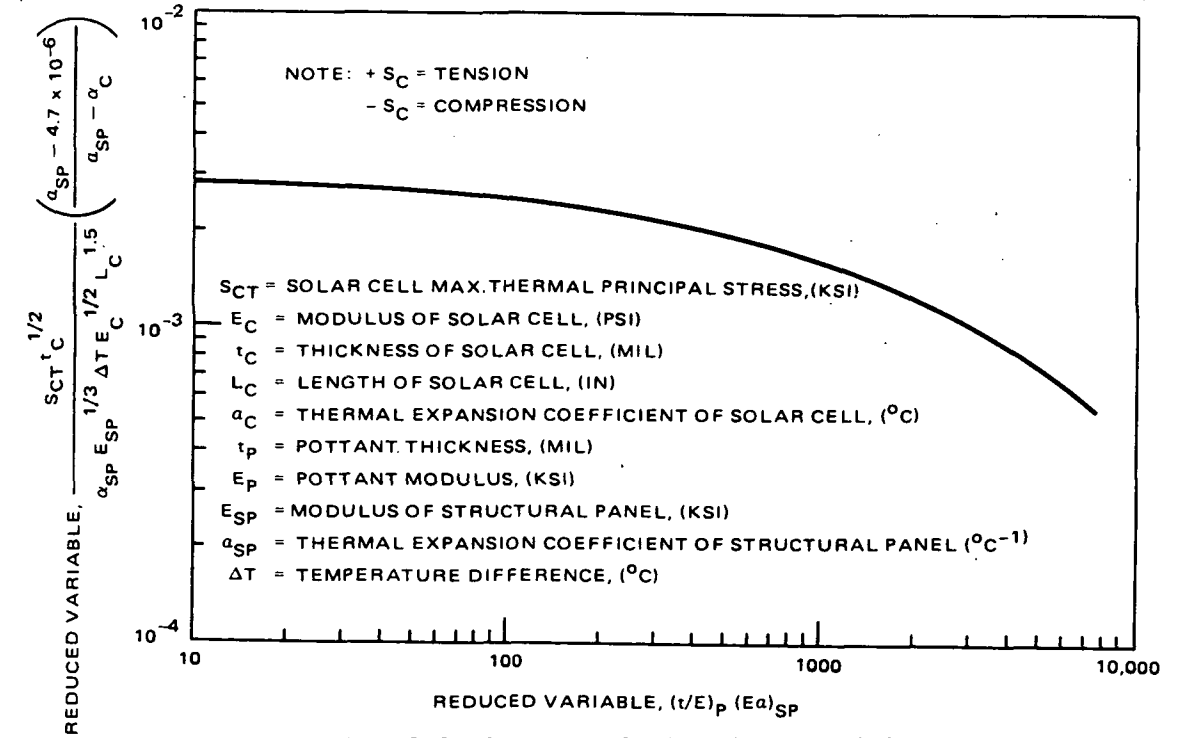

Figure 3-3. Master curve for thermal stress analysis.

where

S_{CT} = SOLAR CELL MAXIMUM PRINCIPAL THERMAL STRESS
E_C = MODULUS OF SOLAR CELL
t_C = THICKNESS OF SOLAR CELL
L_C = LENGTH OF SOLAR CELL
a_C = THERMAL EXPANSION COEFFICIENT OF SOLAR CELL
t_P = POTTANT THICKNESS
E_P = POTTANT MODULUS
E_{SP} = MODULUS OF STRUCTURAL PANEL
a_{SP} = THERMAL EXPANSION COEFFICIENT OF STRUCTURAL PANEL
D_T = TEMPERATURE DIFFERENCE ($T_{CELL}-T_{AMBIENT}$)
a_S = THERMAL EXPANSION COEFFICIENT OF SILICON

As seen in Figure 3-3, the cell stress decreases as the quantity $(t/E)_P\,(E\alpha)_{SP}$ increases.

By comparing equations 1 and 2, it is seen that solar cell stress due to thermal loading is dependent upon many of the variables which are important for pressure loading. Although some of the exponents are slightly different, changes in the parameters produce similar changes in cell stress, regardless of the type of loading. For example, for either thermal or pressure loading, cell stress increases when the cell thickness is decreased or when the pottant thickness is decreased.

Thermal stress in the cell occurs when there is a mismatch of coefficients of thermal expansion of the structural panel and the cell, $\alpha_{SP} \neq \alpha_C$, and a temperature change, ΔT, from ambient. If the coefficient of expansion of the cell is less than that of the structural panel an increase in module temperature generates tension in the cell, and a decrease in module temperature generates compression in the cell. The condition is reversed if the coefficient of thermal expansion of the cell is greater than that of the structural panel.

3.2 PARAMETER LIMITS

The computer analyses from which the master curves were derived encompassed the following parameter ranges.

Structural Panel

E_{SP}: 0.75 - 30 MSI
t_{SP}: 0.04 - 0.25 in.
α_{SP}: 7 - 24 μin/in/°C

Pottant

E_P: 0.5 - 2.5 KSI

t_P: 0.001 - 0.020 in.

Cell

E_C: 5 - 30 MSI

t_C: 0.005 - 0.015 in.

α_C: 1 - 12 μin/in/°C

L_C: 1 - 4 in.

In general, these limits can be increased or halved by a factor of two without degrading the accuracy. Cell thickness should not be less than 2-3 mils because the master curves have not been verified for thin-film solar cells.

3.3 COMBINED PRESSURE AND THERMAL LOADING

When a module is subjected to simultaneous temperature and pressure loading, the resultant cell stresses should be combined according to the following criterion (Reference 5):

$$\frac{\sigma_P + \sigma_T}{\sigma_{BT}} \leq 1.0 \tag{3}$$

where

σ_P = cell stress due to pressure loading (same as S_{CP})

σ_T = cell stress due to thermal loading (same as S_{CT})

σ_{BT} = cell breaking stress

The design is adequate if the computed ratio is less than or equal to 1.0. If it is greater than 1.0, cell failure may occur.

4.0 SAMPLE PROBLEM

The following design problem demonstrates the use of the master curves.

Loading: $\Delta T = 100$ °C
wind pressure = 50 PSF

Structural Panel: Glass

$E_{SP} = 10 \times 10^6$ PSI

$t_{SP} = 0.125$ in.

$\alpha_{SP} = 9.2 \times 10^{-6}$ in/in/°C

S_{SP} = 6 KSI (Determined from a separate analysis of the structural panel)

Pottant: EVA

E_P = 1 KSI

t_P = 5 mil

Solar Cell: Silicon, 4 in × 4 in × 0.010 in

E_C = 17 × 10^6 PSI

t_C = 10 mil

α_C = 4.7 × 10^{-6} in/in/°C

L_C = 4 in

A. Pressure Stress Analysis

Solar cell stress for pressure loading is computed from Figure 3-1, the master curve for pressure stress analysis.

STEP 1: Compute the value of the abscissa.

$$(t/E)_P \left(\frac{1}{Et^3}\right)_{SP} = \left(\frac{5\ \text{MIL}}{1\ \text{KSI}}\right)\left(\frac{1}{(10 \times 10^6\ \text{PSI})\ (0.125\ \text{IN})^3}\right) = 2.56 \times 10^{-4}$$

STEP 2: Enter Figure 3-1. For 50 PSF pressure loading, use curve B. The value of the ordinate is

$$\frac{S_{CP}\ E_{SP}\ t_{SP}\ t_P^{1/8}\ t_C^{1/3}}{S_{SP}\ E_C^{1/2}\ L_C^{1.15}} \doteq 9 \times 10^1$$

Rearranging terms,

$$S_{CP} = \frac{(9 \times 10^1)\ S_{SP}\ E_C^{1/2}\ L_C^{1.15}}{E_{SP}\ t_{SP}\ t_P^{1/8}\ t_C^{1/3}}$$

or,

$$S_{CP} = \frac{(9 \times 10^1)\ (6\ \text{KSI})\ (17 \times 10^6\ \text{PSI})^{1/2}\ (4\ \text{IN})^{1.15}}{(10 \times 10^6\ \text{PSI})\ (0.125\ \text{IN})\ (5\ \text{MIL})^{1/8}\ (10\ \text{MIL})^{1/3}}$$

$\therefore$ S_{CP} = 3.33 KSI

B. Thermal Stress Analysis

Solar cell stress for thermal loading is computed from Figure 3-3, the master curve for thermal stress analysis.

STEP 1: Compute the value of the abscissa.

$$(t/E)_P(E\alpha)_{SP} = \left(\frac{5\ \text{MIL}}{1\ \text{KSI}}\right)\left((10 \times 10^6\ \text{PSI})\,(9.2 \times 10^{-6}\ °\text{C}^{-1})\right) = 460$$

STEP 2: Enter Figure 3-2. The value of the ordinate is

$$\frac{S_C\, t_C^{1/2}}{\alpha_{SP}\, E_{SP}^{1/3}\, \Delta T\, E_C^{1/2}\, L_C^{1.5}} \left(\frac{\alpha_{SP} - 4.7 \times 10^{-6}}{\alpha_{SP} - \alpha_C}\right) \doteq 2 \times 10^{-3}$$

Rearranging terms,

$$S_{CT} = (2 \times 10^{-3})\, \frac{\alpha_{SP}\, E_{SP}^{1/3}\, \Delta T\, E_C^{1/2}\, L^{1.5}}{t_C^{1/2}} \left(\frac{\alpha_{SP} - \alpha_C}{\alpha_{SP} - 4.7 \times 10^{-6}}\right)$$

or,

$$S_{CT} = \frac{(2 \times 10^{-3})\,(9.2 \times 10^{-6}\ °\text{C}^{-1})\,(10 \times 10^6\ \text{PSI})^{1/3}\,(100°\text{C})\,(17 \times 10^6\ \text{PSI})^{1/2}\,(4\ \text{IN})^{1.5}}{(10\ \text{MIL})^{1/2}}$$

$$\left(\frac{(9.2 \times 10^{-6} - 4.7 \times 10^{-6})\ °\text{C}^{-1}}{(9.2 \times 10^{-6} - 4.7 \times 10^{-6})\ °\text{C}^{-1}}\right)$$

$\therefore$ $S_{CT} = 4.13$ KSI

C. Combined Loading Analysis

Cell stresses due to simultaneous pressure and thermal loading are combined according to Equation 3:

$$\frac{\sigma_P + \sigma_T}{\sigma_{BT}} \leq 1.0$$

where

σ_P = cell stress due to wind pressure = 3330 PSI
σ_T = cell stress due to thermal excursion = 4130 PSI
σ_{BT} = cell breaking stress = 5000 PSI, silicon (Reference 1)

$$\frac{\sigma_P + \sigma_T}{\sigma_{BT}} = \frac{3330 + 4130}{5000} = 1.5$$

$$1.5 > 1.0$$

Conclusion: Cell fracture may occur
Recommendation: Increase pottant thickness

5.0 RECOMMENDATIONS

The analytical models should be extended to accommodate thin-film solar cell technology. This can be accomplished as follows:

1. Extend the cell thickness parameter range to cells thinner than 1 mil. Currently, the analytical models are not recommended for a cell thickness less than 2-3 mils.
2. Extend the cell length parameter range to cells as long as 12 inches. Thin-film devices are currently being produced in strips or panels up to 12 inches long. The existing analytical models have not been verified for lengths greater than 4 inches.

ACKNOWLEDGEMENTS

The author would like to thank the following individuals for the many helpful suggestions and technical discussions which aided the development of this work: R. E. Holman, I. R. Jones, J. M. Kallis, and C. P. Minning of Hughes Aircraft Company, E. F. Cuddihy, C. D. Coulbert, and D. M. Moore of the Jet Propulsion Laboratory, and A. Garcia of Spectrolab, Inc. The author also wishes to thank K.O. Ng and S.D. Lust of Hughes Aircraft Company for their assistance with the computer analyses.

REFERENCES

1. Hughes Aircraft Co., "Design, Analysis, and Test Verification of Advanced Encapsulation Systems-Phase 1 Interim Report," Spectrolab Letter Contract #79PMY2636321/88774.
2. Hughes Aircraft Co., "Analysis and Test Verification of Encapsulation Systems for Terrestrial Photovoltaic Modules—Phase 2 Interim Report." Spectrolab Letter Contract #79PMY2636321/88774.
3. Cuddihy, E.F., "Development of Reduced—Variable Master Curves for Estimating Tensile Stresses of Encapsulated Solar Cells caused by Module Deflection or Thermal Expansion," JPL Report 5101-182, October 1, 1981.
4. Roark, R.J., "Formulas for Stress and Strain," McGraw Hill Book Company, Fourth Edition, 1965.
5. Moore, D.M., "Low-Cost Solar Array Project Proposed Method for Determining the Thickness of Glass in Solar Collector Panels," JPL Report 5101-148, 1 March 1980.

APPENDIX C

OPTICAL ANALYSIS

James F. Coakley
Hughes Aircraft Company
El Segundo, California

March, 1983

TABLE OF CONTENTS

LIST OF ILLUSTRATIONS

LIST OF TABLES

SUMMARY

The present report presents the results of the Phase III A & B optical tasks as defined in Reference 1 and Encapsulation Design Letter Reports for the period September, 1983 through January, 1983. Earlier analysis considered the complete photovoltaic module over a wide range of encapsulation designs, materials and cells with the power output as the result of primary interest. The present studies, prompted by recent developments in the LSSA Project, were designed to extend and expand on the earlier optical analysis by providing detailed information not previously available to the designer. Tables and graphs are provided as design tools to aid the module designer in material selection. While no single table or figure considers the complete problem, they do address significant portions of the overall problem and thus permit trends to be established.

However, further optical analytical work is warranted, because the only tool presently available for evaluating configurations not analyzed herein is the large computer program developed in the first phase of the present study. Few designers have a comparable code or wish to spend the time required to learn to use one. Master curves or a computational algorithm which can be exercised easily and which are readily available would be a powerful tool for the designer. Such tools would free the designer from the need to have access to a large computer for module evaluations.

Therefore it is recommended that optical master curves (direct radiation, normal incidence) or a computational algorithm, which would permit the calculation of energy absorbed in the cell and encapsulant layers, be developed. These curves should include the influence of thin film AR coatings and permit calculations to be made as a function of wavelength. The curves could thus be used in evaluations of aging effects on module performance. Also, it seems reasonable to expect that this effort would form the basis for a similar development in the promising area of thin film optical stacks used in advanced module designs.

1.0 INTRODUCTION

1.1 BACKGROUND

Earlier work, reported in Reference 2, considered a wide range of encapsulation designs, materials and cells. This work was accomplished through the use of a thermal-optical computer program which incorporated the optical relations as a subroutine in the program. The materials considered were those commercially available and had indices of refraction of 1.4 to 1.5 for both cover and pottant. Energy absorbed as well as temperature dependence of cell conversion efficiency was considered explicitly.

1.2 PRESENT INVESTIGATION

In the present work, the following areas and their influence on cell performance are investigated in detail:

- Cell Type
  - Single Crystal
  - Polycrystalline
  - Amporphous
- Anti-Reflective (AR) Coating
  - Coated
  - Uncoated
- Refractive Index
  - Cover
  - Pottant
  - AR Coating
- Solar Spectrum

The ranges of cover and pottant indices of refraction are extended to establish data for contour plots and tables with power output and module conversion efficiency as the dependent variables. The influences of the AR coating thickness and refractive index on power output are also considered. Finally, two techniques for subdividing the solar spectrum are considered. The first treats equal-width wavelength intervals while the second treats intervals with equal energy content. Tables based on these techniques were prepared to permit calculations of a low, intermediate or high degree of resolution or accuracy.

2.0 ANALYSIS

2.1 DESCRIPTION OF PROBLEM

A single cell is considered as in Reference 2. The cell is single crystal, polycrystalline or amorphous and is 10.2 cm square with a 0.13 cm intercell space. The cell is subjected to AM 1.5 sunlight with a tilt of 37^{o}. The wind speed, module front and back side radiative properties, encapsulant material and thickness are such that a cell temperature of $50^{o}C$ is achieved. In the present work, the absorption in the cover and pottant layers is taken as zero. The temperature-related cell conversion efficiency was calculated based on the cell temperature of $50^{o}C$ noted previously.

2.2 METHOD

For normal incidence Fresnel's equation can be expressed as

$$\rho = \left(\frac{N_1 - N_2}{N_1 + N_2} \right)^2$$

This relationship is used to calculate reflectance at the interface between media 1 and 2. In the earlier work the reflectance at the cover-air interface was measured as a function of wavelength while internal reflections were calculated using the above expression. Reflections at texturized and AR-coated cell surfaces are treated as described in Reference 2. The thickness of all AR-coatings was chosen to result in a minimum reflectivity at a wavelength of 0.6 micron.

The data presented in this paper were calculated using an extended version of the optical subroutine mentioned in Section 1.1. This subroutine makes use of the net radiation technique and equal energy intervals (Reference 2) in order to calculate the energy transmitted to the cell surface in an optical stack including cover, pottant and AR coating above the solar cell.

3.0 DISCUSSION OF RESULTS

3.1 CELL PERFORMANCE - PARAMETER STUDY

Data have been generated for the following fourteen configurations of single crystal cells (one for each of the two uncoated cells and one for each of the coating refractive indices with the two coated cells):

- Plain silicon.
- Texturized, non AR-coated silicon.
- Plain, AR-coated silicon with coating indices of refraction = 2.0, 2.2, 2.4, 2.6, 2.8, and 3.0.
- Texturized, AR-coated with coating indices of refraction = 2.0, 2.2, 2.4, 2.6, 2.8, and 3.0.

For each configuration, two tables have been prepared - one showing the module power output as a function of the cover and pottant refractive indices and the other showing the module power conversion efficiency as a function of these refractive indices. These 28 tables are presented in Appendix A.

The results for two typical configurations - the plain cell with coating refractive indices = 2.2 and 2.4 - are discussed below. Tables 1 and 2 (the same as Tables A-12A and A-13A of Appendix A) show the module conversion efficiency for a single-crystal cell for two values of AR-coating index of refraction: 2.2 and 2.4, respectively. Figures 1 and 3, contour plots based on Tables 1 and 2, show contours of constant module conversion efficiency versus pottant and cover index of refraction. As expected, the maximum conversion efficiency shifts to higher values of pottant and cover indices with increasing AR-coating index. Since absorption in the cover and pottant layers is neglected, this results in an increase in the energy available for conversion to electrical output.

Absorption was taken into account in the results of Reference 2 from which a representative conversion efficiency of 0.129 was obtained. This is 0.006 lower than the corresponding value of 0.135 taken from Tables 1 and 2. As an approximation, one can assume that 4% of the incident flux is absorbed in the cover and pottant layers. With a single-crystal cell conversion efficiency of 0.145, the decrease in performance would be about (0.04)(0.145) = 0.0058, a value in close agreement with the 0.006 difference noted previously.

TABLE 1. MODULE POWER CONVERSION EFFICIENCY AT AM 1.5, AR COATING REFRACTIVE INDEX = 2.2

		COVER INDEX OF REFRACTION										
		1.0	1.1	1.2	1.3	1.4	1.5	1.6	1.7	1.8	1.9	2.0
	1.0	0.134	0.134	0.132	0.130	0.128	0.125	0.122	0.118	0.115	0.112	0.109
	1.1	0.136	0.136	0.135	0.134	0.131	0.129	0.126	0.123	0.120	0.116	0.113
	1.2	0.137	0.138	0.137	0.136	0.134	0.131	0.129	0.126	0.123	0.120	0.117
POTTANT	1.3	0.137	0.138	0.138	0.137	0.135	0.133	0.131	0.128	0.125	0.122	0.119
INDEX	1.4	0.136	0.138	0.138	0.137	0.136	0.134	0.132	0.130	0.127	0.124	0.121
OF	1.5	0.135	0.137	0.137	0.137	0.136	0.135	0.133	0.130	0.128	0.125	0.123
REFRACTION	1.6	0.133	0.135	0.136	0.136	0.136	0.134	0.133	0.131	0.128	0.126	0.123
	1.7	0.130	0.133	0.134	0.135	0.135	0.134	0.132	0.130	0.128	0.126	0.124
	1.8	0.128	0.131	0.132	0.133	0.133	0.132	0.131	0.130	0.128	0.126	0.124
	1.9	0.125	0.128	0.130	0.131	0.131	0.131	0.130	0.129	0.127	0.125	0.123
	2.0	0.123	0.126	0.128	0.129	0.130	0.129	0.129	0.128	0.126	0.124	0.123

TABLE 2. MODULE POWER CONVERSION EFFICIENCY AT AM 1.5, AR COATING REFRACTIVE INDEX = 2.4

		COVER INDEX OF REFRACTION										
		1.0	1.1	1.2	1.3	1.4	1.5	1.6	1.7	1.8	1.9	2.0
	1.0	0.131	0.131	0.129	0.127	0.125	0.122	0.119	0.116	0.113	0.110	0.107
	1.1	0.134	0.134	0.133	0.131	0.129	0.126	0.124	0.121	0.118	0.115	0.112
	1.2	0.136	0.136	0.136	0.134	0.132	0.130	0.127	0.125	0.122	0.119	0.116
POTTANT	1.3	0.136	0.137	0.137	0.136	0.135	0.132	0.130	0.127	0.125	0.122	0.119
INDEX	1.4	0.136	0.137	0.138	0.137	0.136	0.134	0.132	0.130	0.127	0.124	0.121
OF	1.5	0.135	0.137	0.138	0.138	0.137	0.135	0.133	0.131	0.128	0.126	0.123
REFRACTION	1.6	0.134	0.136	0.137	0.137	0.137	0.135	0.134	0.132	0.129	0.127	0.124
	1.7	0.132	0.135	0.136	0.137	0.136	0.135	0.134	0.132	0.130	0.128	0.125
	1.8	0.130	0.133	0.135	0.135	0.135	0.135	0.134	0.132	0.130	0.128	0.126
	1.9	0.128	0.131	0.133	0.134	0.134	0.134	0.133	0.131	0.130	0.128	0.126
	2.0	0.125	0.129	0.131	0.132	0.133	0.133	0.132	0.131	0.129	0.127	0.125

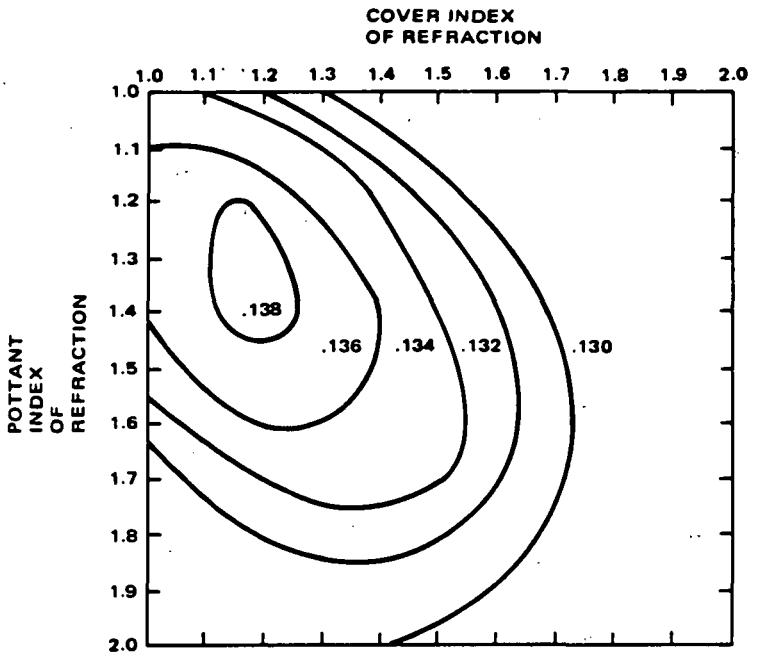

Figure 1. Contours of module conversion efficiency at AM 1.5
AR coating refractive index = 2.2.

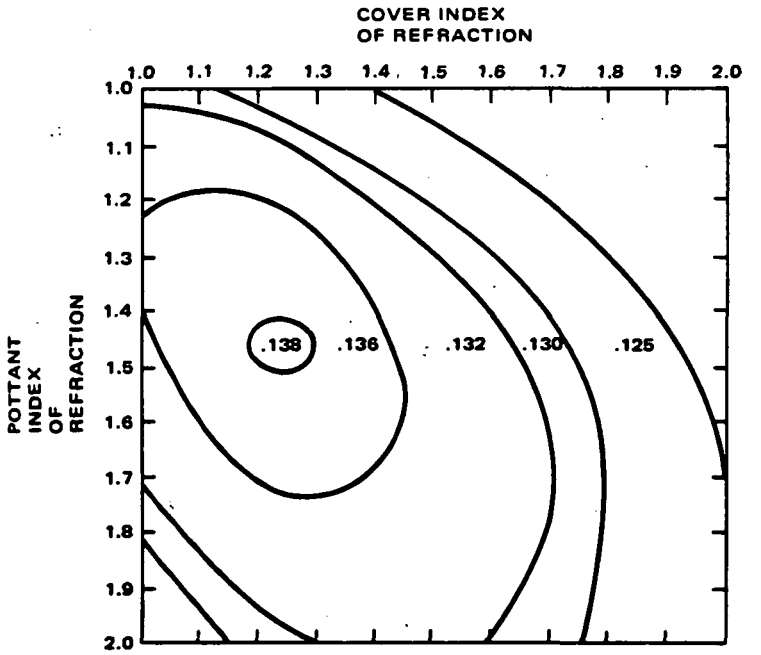

Figure 2. Contours of module conversion efficiency at AM 1.5
AR coating refractive index = 2.4

These optimum cover and pottant refractive indices result from minimization of the over-all reflectance losses. Per Fresnel's equation, these losses result from a mismatch of refractive indices of adjacent layers. Such mismatches are unavoidable, because the air refractive index is 1 and the silicon cell refractive index is 3.73.

The upper left hand entry in Tables 1 and 2 (also in Appendix A) corresponds to the unencapsulated cell case since both cover and pottant indices equal 1. Starting with the upper left hand entry of the tables and moving left to right along the top row, the cover and pottant reflectance increases with a resulting reduction in the power output. When holding the pottant index at a constant value greater than 1 and moving left to right along one of the middle rows, the reflectance at the pottant-cover interface decreases initially, reaching a minimum as the cover and pottant indices approach one another.

3.2 SENSITIVITY OF CELL PERFORMANCE TO AR COATING THICKNESS

Ideally in applying an AR-coating, one would strive for a uniform one-quarter wave-length (optical) thick layer. In practice departures from the ideal occur. Figure 3 was prepared in order to give the reader a feel for the sensitivity of module conversion efficiency with a variation in the actual thickness of the AR-coating layer.

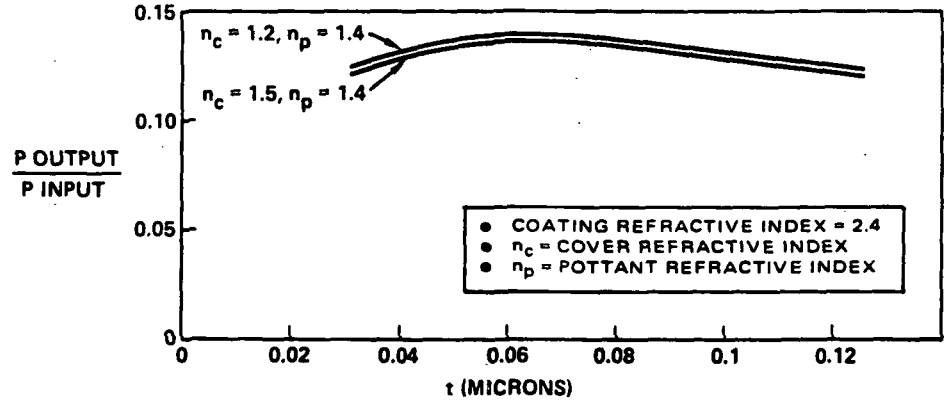

Figure 3. Ratio of power output to power input versus AR coating thickness.

3.3 SOLAR SPECTRAL CALCULATIONS

Two methods of representing the solar irradiation spectrum and material spectral properties are in general use. The first, the equal wavelength interval method, is a straightforward technique quite commonly used in practice. The second method, the equal energy interval method, results in intervals of unequal length whose end points are defined such that the energy in each interval is constant and equal. This is a self normalizing method sometimes referred to as the selected ordinate method.

In the tables to follow, the tabulated quantity is the spectral power output per unit cell area for the spectral band λ_1, λ_2:

$$P_{\lambda_1,\lambda_2} = \int_{\lambda_1}^{\lambda_2} C_\lambda I_\lambda d\lambda$$

where

C_λ = spectral power conversion efficiency of solar cell and
I_λ = spectral solar irradiation

Additionally, the following points should be noted:

- solar cells are bare (unencapsulated)
- cell response data taken from Reference 2
- overall cell conversion efficiency defined as power output/power absorbed. (This contrasts with the typical conversion efficiency, which is defined as power output/incident power.)
- overall cell conversion efficiencies for cells are:

Single-Crystal	16.3%
Polycrystalline	9.6%
Amorphous	5.6%

3.3.1 Equal Wavelength Intervals

Tables 3 through 8 present power output and fraction of power output per wavelength band for single-crystal, poly-crystal and amorphous solar cells. There are six tables organized in groups of two each. The first table of each group presents the power output per wavelength band. The second table presents

TABLE 3.
POWER OUTPUT PER WAVELENGTH BAND (W/M/M)
FROM 0.30 TO 1.20 MICRONS, INTERVAL 0.01 MICRONS
EQUAL WAVELENGTH INTERVALS
(AM1.5 NO AR COATING)

WAVELENGTH	SINGLE CRYSTAL	POLY CRYSTAL	AMORPHOUS	WAVELENGTH	SINGLE CRYSTAL	POLY CRYSTAL	AMORPHOUS
0.305	0.0	0.0	0.0	0.75	3.32	2.03	0.10
0.315	0.0	0.0	0.0	0.76	2.41	1.45	0.05
0.325	0.0	0.0	0.0	0.77	3.14	1.86	0.04
0.335	0.0	0.0	0.0	0.78	3.20	1.88	0.03
0.345	0.0	0.0	0.0	0.79	3.11	1.81	0.02
0.355	0.0	0.0	0.0	0.80	2.84	1.63	0.01
0.365	0.0	0.0	0.0	0.81	2.37	1.35	0.01
0.375	0.03	0.01	0.07	0.82	2.74	1.55	0.0
0.385	0.10	0.04	0.18	0.83	2.67	1.49	0.0
0.395	0.20	0.08	0.35	0.84	2.79	1.54	0.0
0.405	0.37	0.15	0.62	0.85	2.75	1.50	0.0
0.415	0.53	0.21	0.90	0.86	2.70	1.45	0.0
0.425	0.67	0.30	1.04	0.87	2.64	1.40	0.0
0.435	0.88	0.44	1.20	0.88	2.35	1.24	0.0
0.445	1.20	0.64	1.49	0.89	1.86	0.97	0.0
0.455	1.62	0.90	1.87	0.90	1.68	0.87	0.0
0.465	1.98	1.14	2.17	0.91	1.77	0.91	0.0
0.475	2.22	1.32	2.32	0.92	1.88	0.96	0.0
0.485	2.41	1.46	2.42	0.93	0.59	0.30	0.0
0.495	2.57	1.60	2.49	0.94	1.09	0.54	0.0
0.505	2.79	1.77	2.60	0.95	0.77	0.38	0.0
0.515	2.90	1.88	2.62	0.96	1.28	0.62	0.0
0.525	3.00	2.00	2.62	0.97	1.38	0.65	0.0
0.535	3.08	2.10	2.61	0.98	1.46	0.66	0.0
0.545	3.09	2.13	2.52	0.99	1.50	0.65	0.0
0.555	3.06	2.10	2.39	1.00	1.41	0.58	0.0
0.565	2.99	2.05	2.24	1.01	1.31	0.50	0.0
0.575	2.96	2.03	2.13	1.02	1.22	0.43	0.0
0.585	2.97	2.05	2.06	1.03	1.13	0.36	0.0
0.595	3.02	2.12	2.02	1.04	1.02	0.31	0.0
0.605	3.14	2.23	2.02	1.05	0.90	0.27	0.0
0.615	3.21	2.28	1.88	1.06	0.79	0.24	0.0
0.625	3.24	2.28	1.63	1.07	0.65	0.20	0.0
0.635	3.29	2.29	1.39	1.08	0.49	0.15	0.0
0.645	3.35	2.31	1.17	1.09	0.35	0.10	0.0
0.655	3.41	2.33	0.99	1.10	0.22	0.06	0.0
0.665	3.46	2.35	0.85	1.11	0.10	0.03	0.0
0.675	3.37	2.27	0.68	1.12	0.04	0.01	0.0
0.685	3.11	2.09	0.50	1.13	0.01	0.0	0.0
0.695	3.10	2.06	0.39	1.14	0.02	0.0	0.0
0.705	3.34	2.18	0.35	1.15	0.01	0.0	0.0
0.715	2.88	1.86	0.24	1.16	0.02	0.0	0.0
0.725	2.62	1.67	0.16	1.17	0.02	0.0	0.0
0.735	3.07	1.92	0.15	1.18	0.02	0.0	0.0
0.745	3.30	2.04	0.13	1.19	0.02	0.0	0.0

TABLE 4.

FRACTION OF POWER OUTPUT PER WAVELENGTH BAND
FROM 0.30 TO 1.20 MICRONS, INTERVAL 0.01 MICRONS
EQUAL WAVELENGTH INTERVALS
(AM1.5 NO AR COATING)

WAVELENGTH	SINGLE CRYSTAL	POLY CRYSTAL	AMORPHOUS	WAVELENGTH	SINGLE CRYSTAL	POLY CRYSTAL	AMORPHOUS
0.305	0.0	0.0	0.0	0.755	0.021	0.022	0.002
0.315	0.0	0.0	0.0	0.765	0.015	0.015	0.001
0.325	0.0	0.0	0.0	0.775	0.020	0.020	0.001
0.335	0.0	0.0	0.0	0.785	0.020	0.020	0.001
0.345	0.0	0.0	0.0	0.795	0.020	0.019	0.0
0.355	0.0	0.0	0.0	0.805	0.018	0.017	0.0
0.365	0.0	0.0	0.0	0.815	0.015	0.014	0.0
0.375	0.000	0.000	0.001	0.825	0.017	0.017	0.0
0.385	0.001	0.000	0.003	0.835	0.017	0.016	0.0
0.395	0.001	0.001	0.006	0.845	0.018	0.016	0.0
0.405	0.002	0.002	0.012	0.855	0.018	0.016	0.0
0.415	0.003	0.002	0.017	0.865	0.017	0.016	0.0
0.425	0.004	0.003	0.019	0.875	0.017	0.015	0.0
0.435	0.006	0.005	0.022	0.885	0.015	0.013	0.0
0.445	0.008	0.007	0.028	0.895	0.012	0.010	0.0
0.455	0.010	0.010	0.035	0.905	0.011	0.009	0.0
0.465	0.013	0.012	0.040	0.915	0.011	0.010	0.0
0.475	0.014	0.014	0.043	0.925	0.012	0.010	0.0
0.485	0.015	0.016	0.045	0.935	0.004	0.003	0.0
0.495	0.016	0.017	0.046	0.945	0.007	0.006	0.0
0.505	0.018	0.019	0.048	0.955	0.005	0.004	0.0
0.515	0.019	0.020	0.049	0.965	0.008	0.007	0.0
0.525	0.019	0.021	0.049	0.975	0.009	0.007	0.0
0.535	0.020	0.022	0.049	0.985	0.009	0.007	0.0
0.545	0.020	0.023	0.047	0.995	0.010	0.007	0.0
0.555	0.020	0.022	0.044	1.005	0.009	0.006	0.0
0.565	0.019	0.022	0.042	1.015	0.008	0.005	0.0
0.575	0.019	0.022	0.040	1.025	0.008	0.005	0.0
0.585	0.019	0.022	0.038	1.035	0.007	0.004	0.0
0.595	0.019	0.023	0.038	1.045	0.007	0.003	0.0
0.605	0.020	0.024	0.037	1.055	0.006	0.003	0.0
0.615	0.021	0.024	0.035	1.065	0.005	0.003	0.0
0.625	0.021	0.024	0.030	1.075	0.004	0.002	0.0
0.635	0.021	0.024	0.026	1.085	0.003	0.002	0.0
0.645	0.021	0.025	0.022	1.095	0.002	0.001	0.0
0.655	0.022	0.025	0.018	1.105	0.001	0.001	0.0
0.665	0.022	0.025	0.016	1.115	0.001	0.0	0.0
0.675	0.021	0.024	0.013	1.125	0.0	0.0	0.0
0.685	0.020	0.022	0.009	1.135	0.0	0.0	0.0
0.695	0.020	0.022	0.007	1.145	0.0	0.0	0.0
0.705	0.021	0.023	0.007	1.155	0.0	0.0	0.0
0.715	0.018	0.020	0.004	1.165	0.0	0.0	0.0
0.725	0.017	0.018	0.003	1.175	0.0	0.0	0.0
0.735	0.020	0.021	0.003	1.185	0.0	0.0	0.0
0.745	0.021	0.022	0.002	1.195	0.0	0.0	0.0

TABLE 5.
POWER OUTPUT PER WAVELENGTH BAND (W/M/M)
FROM 0.30 TO 1.20 MICRONS, INTERVAL 0.05 MICRONS
EQUAL WAVELENGTH INTERVALS
(AM1.5 NO AR COATING)

WAVELENGTH	SINGLE CRYSTAL	POLY CRYSTAL	AMORPHOUS	WAVELENGTH	SINGLE CRYSTAL	POLY CRYSTAL	AMORPHOUS
0.325	0.0	0.0	0.0	0.775	15.18	9.03	0.24
0.375	0.33	0.13	0.60	0.825	13.41	7.56	0.02
0.425	3.65	1.74	5.25	0.875	12.30	6.56	0.0
0.475	10.80	6.42	11.27	0.925	7.01	3.58	0.0
0.525	14.86	9.88	12.97	0.975	6.39	2.96	0.0
0.575	15.00	10.35	10.84	1.025	6.09	2.18	0.0
0.625	16.23	11.39	8.09	1.075	3.18	0.96	0.0
0.675	16.45	11.10	3.41	1.125	0.39	0.10	0.0
0.725	15.21	9.67	1.03	1.175	0.09	0.0	0.0

TABLE 6.
FRACTION OF POWER OUTPUT PER WAVELENGTH BAND
FROM 0.30 TO 1.20 MICRONS, INTERVAL 0.05 MICRONS
EQUAL WAVELENGTH INTERVALS
(AM1.5 NO AR COATING)

WAVELENGTH	SINGLE CRYSTAL	POLY CRYSTAL	AMORPHOUS	WAVELENGTH	SINGLE CRYSTAL	POLY CRYSTAL	AMORPHOUS
0.325	0.0	0.0	0.0	0.775	0.096	0.096	0.005
0.375	0.002	0.001	0.010	0.825	0.085	0.08	0.0
0.425	0.023	0.019	0.098	0.875	0.079	0.07	0.0
0.475	0.068	0.069	0.209	0.925	0.045	0.038	0.0
0.525	0.096	0.105	0.242	0.975	0.041	0.032	0.0
0.575	0.096	0.111	0.202	1.025	0.039	0.023	0.0
0.625	0.102	0.121	0.150	1.075	0.020	0.011	0.0
0.675	0.105	0.118	0.063	1.125	0.002	0.001	0.0
0.725	0.097	0.104	0.019	1.175	0.0	0.0	0.0

TABLE 7.
POWER OUTPUT PER WAVELENGTH BAND (W/M/M)
FROM 0.30 TO 1.20 MICRONS, INTERVAL 0.10 MICRONS
EQUAL WAVELENGTH INTERVALS
(AM1.5 NO AR COATING)

WAVELENGTH	SINGLE CRYSTAL	POLY CRYSTAL	AMORPHOUS	WAVELENGTH	SINGLE CRYSTAL	POLY CRYSTAL	AMORPHOUS
0.350	0.33	0.13	0.6	0.850	25.71	14.12	0.02
0.450	14.45	8.16	16.52	0.950	13.4	6.54	0.0
0.550	29.86	20.23	23.81	1.050	9.27	3.14	0.0
0.650	32.68	22.49	11.5	1.150	0.48	0.1	0.0
0.750	30.39	18.7	1.27				

TABLE 8.
FRACTION OF POWER OUTPUT PER WAVELENGTH BAND
FROM 0.30 TO 1.20 MICRONS, INTERVAL 0.10 MICRONS
EQUAL WAVELENGTH INTERVALS
(AM1.5 NO AR COATING)

WAVELENGTH	SINGLE CRYSTAL	POLY CRYSTAL	AMORPHOUS	WAVELENGTH	SINGLE CRYSTAL	POLY CRYSTAL	AMORPHOUS
0.350	0.002	0.001	0.01	0.850	0.164	0.15	0.0
0.450	0.091	0.088	0.307	0.950	0.056	0.07	0.0
0.550	0.192	0.216	0.444	1.050	0.059	0.034	0.0
0.650	0.209	0.239	0.213	1.150	0.002	0.001	0.0
0.750	0.193	0.20	0.024	0.0			

the fraction of power output per wavelength band. All tables cover the wavelength interval from 0.3 to 1.2 microns. This interval encompasses the solar cell response range. Depending on the degree of resolution or accuracy required, one would use Tables 3 and 4 (greatest resolution), Tables 5 and 6 (intermediate resolution) or Tables 7 and 8 (nine points-lowest resolution).

Figures 4, 5 and 6 are bar charts (taken from Table 6) of percent power output versus wavelength for single-crystal, polycrystalline and amorphous solar cells, respectively. The figures emphasize the wavelength regions over which the intensity-response product is greatest. The charts clearly show

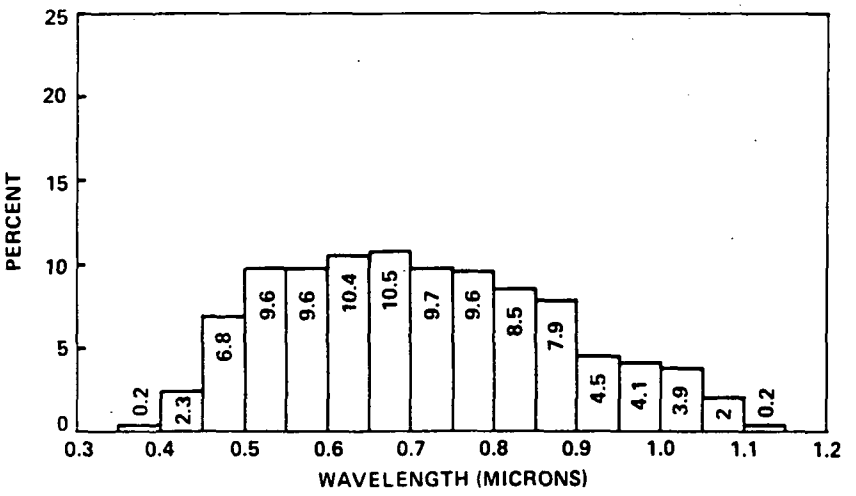

Figure 4. Spectral contributions to power output — single-crystal cell.

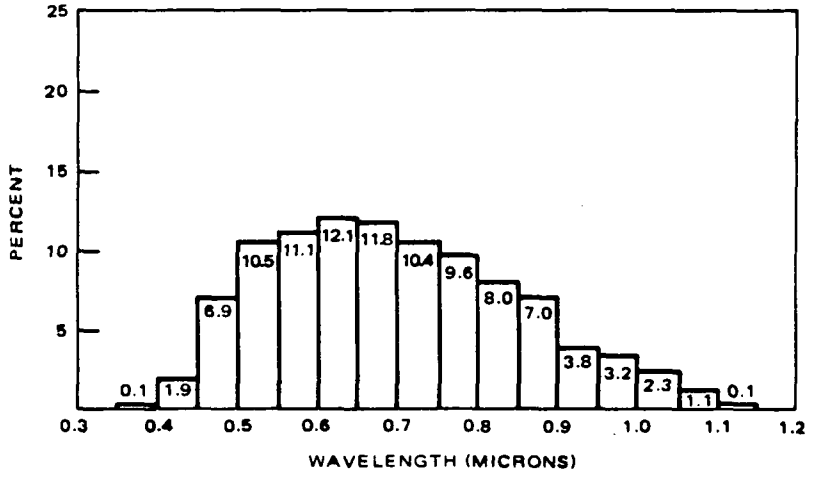

Figure 5. Spectral contributions to power output-polycrystalline cell.

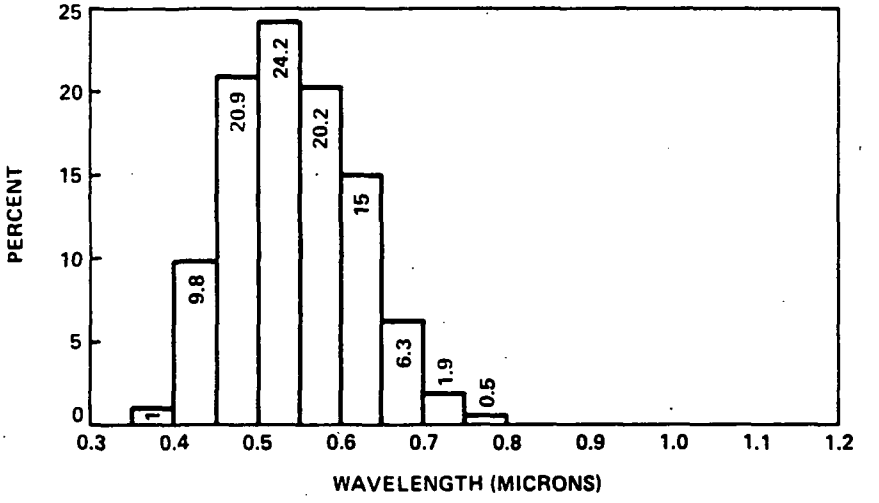

Figure 6. Spectral contributions to power output — amorphous cell.

that the single-crystal and polycrystalline cells make better use of the entire solar intensity spectrum than does the amorphous cell. The magnitude of the power output per wavelength band for these figures is presented in Table 5. Although the percent power output charts for single-crystal and polycrystalline cells, Figures 4 and 5 respectively, are comparable, Table 5 shows that the magnitude of the single-crystal cell is about 68 percent greater than the magnitude of the polycrystalline cell. The strength or magnitude of the single-crystal cell response combined with a wide region of response result in a high overall cell conversion efficiency. Figure 7 shows a continuous plot of Figure 4, the single-crystal intensity-response product, as well as the transmittance of a typical pottant, EVA/Craneglas. Although just one component in the determination of the actual transmittance to the cell surface, the inclusion of the pottant transmittance curve shows the importance of the careful selection of pottant materials. The transmittance curve reaches a peak transmittance value and maintains this value throughout the useful region of the intensity-response curve. The transmittance curve was obtained by measuring reflectance/transmittance through a 20 mil thick specimen of EVA/Craneglas.

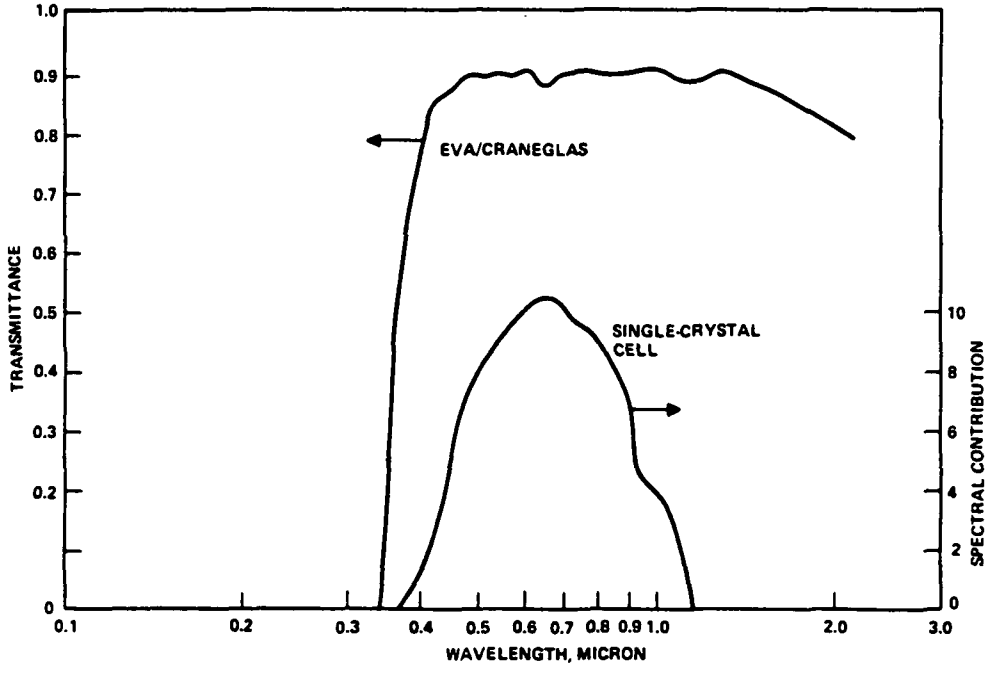

Figure 7. Relation between spectral contributions to power output and pottant transmission spectrum.

3.3.2 Equal Energy Intervals

Tables 9 through 14 make use of the same data base as that used in Section 3.3.1 except that equal energy intervals rather than wavelength intervals are used. The organization of these tables is identical to that of Section 3.3.1. This method was the method chosen for use in the first phase of the work summarized in Reference 2. The number of intervals considered (resolution) ranges from 100 to 20 while the entire solar spectrum is covered.

TABLE 9.
POWER OUTPUT PER ENERGY BAND (W/M/M)
FROM 0.30 TO 2.45 MICRONS, INTERVAL -100
EQUAL ENERGY INTERVALS
(AM1.5 NO AR COATING)

WAVELENGTH	SINGLE CRYSTAL	POLY CRYSTAL	AMORPHOUS	WAVELENGTH	SINGLE CRYSTAL	POLY CRYSTAL	AMORPHOUS
0.331	0.0	0.0	0.0	0.712	2.83	1.83	0.25
0.351	0.0	0.0	0.0	0.722	2.95	1.89	0.20
0.367	0.0	0.0	0.0	0.731	2.74	1.73	0.14
0.382	0.11	0.04	0.20	0.741	2.94	1.83	0.13
0.395	0.24	0.09	0.41	0.749	2.83	1.74	0.10
0.405	0.35	0.14	0.60	0.758	3.21	1.95	0.09
0.414	0.43	0.17	0.73	0.769	3.05	1.83	0.06
0.422	0.51	0.21	0.83	0.778	2.95	1.74	0.03
0.430	0.59	0.28	0.86	0.787	2.92	1.71	0.02
0.438	0.72	0.36	0.95	0.796	2.99	1.74	0.02
0.445	0.82	0.44	1.02	0.806	2.90	1.67	0.01
0.452	0.92	0.50	1.08	0.817	2.61	1.49	0.01
0.458	1.02	0.57	1.16	0.829	2.94	1.66	0.0
0.463	1.09	0.62	1.20	0.839	2.94	1.63	0.0
0.469	1.13	0.66	1.21	0.850	2.87	1.58	0.0
0.474	1.20	0.71	1.26	0.860	2.87	1.55	0.0
0.480	1.29	0.77	1.32	0.871	2.88	1.54	0.0
0.485	1.33	0.81	1.34	0.882	3.04	1.60	0.0
0.491	1.38	0.85	1.36	0.895	2.59	1.35	0.0
0.496	1.48	0.92	1.43	0.909	2.48	1.28	0.0
0.502	1.57	0.99	1.48	0.924	3.37	1.71	0.0
0.508	1.64	1.05	1.52	0.945	2.34	1.17	0.0
0.514	1.70	1.10	1.54	0.967	2.44	1.18	0.0
0.520	1.74	1.14	1.55	0.983	2.07	0.95	0.0
0.526	1.80	1.20	1.57	0.996	1.99	0.86	0.0
0.532	1.85	1.25	1.58	1.009	1.81	0.72	0.0
0.538	1.89	1.29	1.59	1.023	1.64	0.60	0.0
0.544	1.92	1.32	1.58	1.036	1.53	0.49	0.0
0.550	2.00	1.37	1.60	1.050	1.37	0.42	0.0
0.557	2.04	1.40	1.58	1.064	1.25	0.38	0.0
0.563	2.01	1.38	1.52	1.081	0.97	0.29	0.0
0.570	2.05	1.40	1.50	1.100	1.01	0.29	0.0
0.577	2.14	1.46	1.52	1.149	0.05	0.0	0.0
0.584	2.14	1.47	1.48	1.181	0.05	0.0	0.0
0.592	2.15	1.49	1.45	1.204	0.03	0.0	0.0
0.599	2.20	1.55	1.45	1.226	0.02	0.0	0.0
0.606	2.26	1.61	1.44	1.249	0.01	0.0	0.0
0.613	2.29	1.63	1.38	1.273	0.0	0.0	0.0
0.620	2.31	1.63	1.25	1.300	0.0	0.0	0.0
0.627	2.34	1.64	1.13	1.357	0.0	0.0	0.0
0.635	2.39	1.66	1.02	1.507	0.0	0.0	0.0
0.642	2.44	1.68	0.90	1.547	0.0	0.0	0.0
0.649	2.48	1.70	0.78	1.585	0.0	0.0	0.0
0.657	2.51	1.71	0.71	1.626	0.0	0.0	0.0
0.664	2.56	1.73	0.64	1.669	0.0	0.0	0.0
0.672	2.67	1.80	0.58	1.719	0.0	0.0	0.0
0.679	2.60	1.75	0.47	1.798	0.0	0.0	0.0
0.687	2.46	1.65	0.37	2.091	0.0	0.0	0.0
0.696	2.56	1.70	0.32	2.211	0.0	0.0	0.0
0.704	2.77	1.82	0.30	2.347	0.0	0.0	0.0

TABLE 10.
FRACTION OF POWER OUTPUT PER ENERGY BAND
FROM 0.30 TO 2.45 MICRONS, INTERVAL -100
EQUAL ENERGY INTERVALS
(AM1.5 NO AR COATING)

WAVELENGTH	SINGLE CRYSTAL	POLY CRYSTAL	AMORPHOUS	WAVELENGTH	SINGLE CRYSTAL	POLY CRYSTAL	AMORPHOUS
0.331	0.0	0.0	0.0	0.712	0.018	0.019	0.005
0.351	0.0	0.0	0.0	0.722	0.019	0.020	0.004
0.367	0.0	0.0	0.0	0.731	0.017	0.018	0.003
0.382	0.001	0.000	0.004	0.741	0.018	0.019	0.002
0.395	0.001	0.001	0.008	0.749	0.018	0.018	0.002
0.405	0.002	0.001	0.011	0.758	0.020	0.021	0.002
0.414	0.003	0.002	0.014	0.769	0.019	0.019	0.001
0.422	0.003	0.002	0.015	0.778	0.018	0.018	0.001
0.430	0.004	0.003	0.016	0.787	0.018	0.018	0.0
0.438	0.005	0.004	0.018	0.796	0.019	0.018	0.0
0.445	0.005	0.005	0.019	0.806	0.018	0.018	0.0
0.452	0.006	0.005	0.020	0.817	0.016	0.016	0.0
0.458	0.006	0.006	0.022	0.829	0.018	0.017	0.0
0.463	0.007	0.007	0.022	0.839	0.018	0.017	0.0
0.469	0.007	0.007	0.023	0.850	0.018	0.017	0.0
0.474	0.008	0.007	0.023	0.860	0.018	0.016	0.0
0.480	0.008	0.008	0.025	0.871	0.018	0.016	0.0
0.485	0.008	0.009	0.025	0.882	0.019	0.017	0.0
0.491	0.009	0.009	0.025	0.895	0.016	0.014	0.0
0.496	0.009	0.010	0.027	0.909	0.016	0.013	0.0
0.502	0.010	0.010	0.027	0.924	0.021	0.018	0.0
0.508	0.010	0.011	0.028	0.945	0.015	0.012	0.0
0.514	0.011	0.012	0.029	0.967	0.015	0.012	0.0
0.520	0.011	0.012	0.029	0.983	0.013	0.010	0.0
0.526	0.011	0.013	0.029	0.996	0.012	0.009	0.0
0.532	0.012	0.013	0.029	1.009	0.011	0.008	0.0
0.538	0.012	0.014	0.030	1.023	0.010	0.006	0.0
0.544	0.012	0.014	0.029	1.036	0.010	0.005	0.0
0.550	0.013	0.014	0.030	1.050	0.009	0.004	0.0
0.557	0.013	0.015	0.029	1.064	0.008	0.004	0.0
0.563	0.013	0.014	0.028	1.081	0.006	0.003	0.0
0.570	0.013	0.015	0.028	1.100	0.006	0.003	0.0
0.577	0.013	0.015	0.028	1.149	0.0	0.0	0.0
0.584	0.013	0.015	0.028	1.181	0.0	0.0	0.0
0.592	0.013	0.016	0.027	1.204	0.0	0.0	0.0
0.599	0.014	0.016	0.027	1.226	0.0	0.0	0.0
0.606	0.014	0.017	0.027	1.249	0.0	0.0	0.0
0.613	0.014	0.017	0.026	1.273	0.0	0.0	0.0
0.620	0.014	0.017	0.023	1.300	0.0	0.0	0.0
0.627	0.015	0.017	0.021	1.357	0.0	0.0	0.0
0.635	0.015	0.018	0.019	1.507	0.0	0.0	0.0
0.642	0.015	0.018	0.017	1.547	0.0	0.0	0.0
0.649	0.016	0.018	0.015	1.585	0.0	0.0	0.0
0.657	0.016	0.018	0.013	1.626	0.0	0.0	0.0
0.664	0.016	0.018	0.012	1.669	0.0	0.0	0.0
0.672	0.017	0.019	0.011	1.719	0.0	0.0	0.0
0.679	0.016	0.018	0.009	1.798	0.0	0.0	0.0
0.687	0.015	0.017	0.007	2.091	0.0	0.0	0.0
0.696	0.016	0.018	0.006	2.211	0.0	0.0	0.0
0.704	0.017	0.019	0.006	2.347	0.0	0.0	0.0

TABLE 11.
POWER OUTPUT PER ENERGY BAND (W/M/M)
FROM 0.30 TO 2.45 MICRONS, INTERVAL -50
EQUAL ENERGY INTERVALS
(AM1.5 NO AR COATING)

WAVELENGTH	SINGLE CRYSTAL	POLY CRYSTAL	AMORPHOUS	WAVELENGTH	SINGLE CRYSTAL	POLY CRYSTAL	AMORPHOUS
0.341	0.0	0.0	0.0	0.717	5.79	3.72	0.45
0.375	0.11	0.04	0.20	0.736	5.68	3.56	0.26
0.401	0.59	0.23	1.01	0.753	6.04	3.69	0.19
0.418	0.95	0.39	1.56	0.773	6.00	3.57	0.09
0.434	1.32	0.64	1.81	0.792	5.90	3.44	0.04
0.448	1.74	0.94	2.11	0.812	5.50	3.15	0.02
0.461	2.11	1.19	2.36	0.834	5.87	3.29	0.00
0.472	2.33	1.37	2.47	0.855	5.74	3.13	0.0
0.482	2.62	1.58	2.65	0.876	5.91	3.13	0.0
0.494	2.86	1.77	2.79	0.901	5.07	2.63	0.0
0.505	3.21	2.04	3.00	0.933	5.72	2.88	0.0
0.517	3.44	2.24	3.09	0.975	4.51	2.13	0.0
0.529	3.64	2.45	3.15	1.003	3.80	1.58	0.0
0.541	3.81	2.62	3.17	1.029	3.17	1.09	0.0
0.553	4.04	2.77	3.18	1.057	2.63	0.80	0.0
0.567	4.06	2.78	3.02	1.090	1.98	0.59	0.0
0.581	4.28	2.93	3.01	1.169	0.10	0.00	0.0
0.595	4.35	3.05	2.90	1.215	0.05	0.0	0.0
0.610	4.55	3.24	2.83	1.261	0.01	0.0	0.0
0.624	4.65	3.27	2.38	1.317	0.0	0.0	0.0
0.638	4.83	3.35	1.92	1.528	0.0	0.0	0.0
0.653	4.98	3.40	1.49	1.605	0.0	0.0	0.0
0.668	5.22	3.54	1.21	1.693	0.0	0.0	0.0
0.683	5.06	3.39	0.84	2.023	0.0	0.0	0.0
0.700	5.34	3.51	0.62	2.276	0.0	0.0	0.0

TABLE 12.

FRACTION OF POWER OUTPUT PER ENERGY BAND
FROM 0.30 TO 2.45 MICRONS, INTERVAL -50
EQUAL ENERGY INTERVALS
(AM1.5 NO AR COATING)

WAVELENGTH	SINGLE CRYSTAL	POLY CRYSTAL	AMORPHOUS	WAVELENGTH	SINGLE CRYSTAL	POLY CRYSTAL	AMORPHOUS
0.341	0.0	0.0	0.0	0.717	0.036	0.039	0.008
0.375	0.001	0.000	0.004	0.736	0.036	0.037	0.005
0.401	0.004	0.002	0.019	0.753	0.038	0.039	0.004
0.418	0.006	0.004	0.029	0.773	0.038	0.038	0.002
0.434	0.008	0.007	0.034	0.792	0.037	0.036	0.001
0.448	0.011	0.010	0.039	0.812	0.034	0.033	0.000
0.461	0.013	0.013	0.044	0.834	0.037	0.035	0.000
0.472	0.015	0.014	0.046	0.855	0.036	0.033	0.0
0.482	0.016	0.017	0.049	0.876	0.037	0.033	0.0
0.494	0.018	0.019	0.052	0.901	0.032	0.028	0.0
0.505	0.020	0.021	0.056	0.933	0.036	0.030	0.0
0.517	0.022	0.024	0.057	0.975	0.028	0.022	0.0
0.529	0.023	0.026	0.059	1.003	0.024	0.017	0.0
0.541	0.024	0.028	0.059	1.029	0.020	0.011	0.0
0.553	0.025	0.029	0.059	1.057	0.016	0.008	0.0
0.567	0.025	0.029	0.056	1.090	0.012	0.006	0.0
0.581	0.027	0.031	0.056	1.169	0.001	0.000	0.0
0.595	0.027	0.032	0.054	1.215	0.000	0.0	0.0
0.610	0.029	0.034	0.053	1.261	0.000	0.0	0.0
0.624	0.029	0.034	0.044	1.317	0.0	0.0	0.0
0.638	0.030	0.035	0.036	1.528	0.0	0.0	0.0
0.653	0.031	0.036	0.028	1.605	0.0	0.0	0.0
0.668	0.033	0.037	0.023	1.693	0.0	0.0	0.0
0.683	0.032	0.036	0.016	2.023	0.0	0.0	0.0
0.700	0.033	0.037	0.012	2.276	0.0	0.0	0.0

TABLE 13.
POWER OUTPUT PER ENERGY BAND (W/M/M)
FROM 0.30 TO 2.45 MICRONS, INTERVAL -20
EQUAL ENERGY INTERVALS
(AM1.5 NO AR COATING)

WAVELENGTH	SINGLE CRYSTAL	POLY CRYSTAL	AMORPHOUS	WAVELENGTH	SINGLE CRYSTAL	POLY CRYSTAL	AMORPHOUS
0.367	0.35	0.14	0.61	0.731	14.30	9.01	0.82
0.422	2.61	1.17	3.97	0.778	15.12	8.97	0.23
0.458	4.98	2.79	5.68	0.829	14.25	8.02	0.02
0.485	6.68	4.07	6.70	0.882	13.85	7.32	0.0
0.514	8.44	5.47	7.65	0.967	12.22	5.87	0.0
0.544	9.70	6.64	7.93	1.036	7.61	2.60	0.0
0.577	10.48	7.20	7.48	1.149	2.12	0.59	0.0
0.613	11.41	8.06	6.65	1.273	0.03	0.0	0.0
0.649	12.37	8.49	4.04	1.585	0.0	0.0	0.0
0.687	13.06	8.71	2.04	2.091	0.0	0.0	0.0

TABLE 14.
FRACTION OF POWER OUTPUT PER ENERGY BAND
FROM 0.30 TO 2.45 MICRONS, INTERVAL -20
EQUAL ENERGY INTERVALS
(AM1.5 NO AR COATING)

WAVELENGTH	SINGLE CRYSTAL	POLY CRYSTAL	AMORPHOUS	WAVELENGTH	SINGLE CRYSTAL	POLY CRYSTAL	AMORPHOUS
0.367	0.002	0.001	0.011	0.731	0.090	0.095	0.015
0.422	0.016	0.012	0.074	0.778	0.095	0.094	0.004
0.458	0.031	0.029	0.105	0.829	0.089	0.084	0.000
0.485	0.042	0.043	0.124	0.882	0.087	0.077	0.0
0.514	0.053	0.058	0.142	0.967	0.077	0.062	0.0
0.544	0.061	0.070	0.147	1.036	0.048	0.027	0.0
0.577	0.066	0.076	0.139	1.149	0.013	0.006	0.0
0.613	0.071	0.085	0.124	1.273	0.000	0.0	0.0
0.649	0.078	0.089	0.075	1.585	0.0	0.0	0.0
0.687	0.082	0.092	0.038	2.091	0.0	0.0	0.0

4.0 RECOMMENDATIONS

It is recommended that optical master curves (direct radiation, normal incidence) or a computational algorithm, which would permit the calculation of energy absorbed in the cell and encapsulant layers, be developed. Master curves or a computational algorithm which can be exercised easily and which are readily available would be a powerful tool for the designer. Such tools would free the designer from the need to have access to a large computer for module evaluations. These curves should include the influence of thin film AR coatings and permit calculations to be made as a function of wavelength. The curves could thus be used in evaluations such as the previously mentioned aging problem. Also, it seems reasonable to expect that this effort would form the basis for a similar development in the promising area of thin film optical stacks used in advanced module designs.

ACKNOWLEDGEMENTS

Technical discussions with C. D. Coulbert, E. F. Cuddihy, A. Garcia, I. R. Jones and J. M. Kallis were very helpful for the work described herein.

REFERENCES

1) Spectrolab Letter Contract No. 79PMY263-6321/88774 Statement of Work, Revision C, Analysis and Definition, 9 April 1982.

2) "Design and Analysis of Advanced Encapsulation System for Terrestrial Photovoltaic Modules", Phase I Topical Report covering work 1 December 1979 to 1 October 1980, Spectrolab Letter Contract No. 79PMY263-6321/88774.

APPENDIX A

MODULE POWER OUTPUT AND CONVERSION EFFICIENCY

Two sets of tables consisting of fourteen tables each were generated to complete the optical tasks of Phase IIIA. The results were generated using input data as specified in the Phase I Report (Reference 2). The first set of tables, Tables A-1 through A-8B, present electrical power output and allow direct comparison with certain entries in Table 6-3 of Reference 2. The second set of tables, Tables A-9 through A-16B, present the module conversion efficiency and have a direct correspondence with the entries in Tables A-1 to A-8. The module conversion efficiency is calculated by dividing the power output by the product of incident flux and cell area.

Tables A-1 through A-8B present electrical power output for AM 1.5 with the integrated incident energy flux taken as 0.114 watts/cm^2 (see footnote page 82, Reference 2). In the Phase I Report the cover index of refraction was about 1.5-1.6 with a pottant index of 1.4. Entering Table A-1 at these indices yields a power output of 1.34 watts. This compares favorably with the output, 1.32 watts, of the superstrate design of Table 6-3, Reference 2 (second entry from top). Similarly entering Table A-2 at these indices results in a power output of 1.52 watts. Again, this compares favorably with the output, 1.47 watts, of the texturized superstrate design of Table 6-3, Reference 2 (ninth entry from top). The last comparisons can be made between data taken from Tables A-4A and A-4B and entries seventeen and eighteen of Table 6-3, Reference 2. These are 1.61 watts versus 1.57 watts for the superstrate design and 1.58 watts versus 1.52 watts for the texturized AR-coated cell-both with an AR coating index of 2.2. The values calculated in the present study are all somewhat higher than the values previously calculated due to a slightly greater amount of energy transmitted to the cell surface in the absence of absorption by the pottant and front cover.

Several conclusions can be drawn from observation of the data in the tables. These are:

- The maximum power output occurs for an AR-coated cell with an index of refraction of 1.3-1.4 and 1.1-1.2 for the pottant and cover layers respectively.

- compared to a bare cell surface, texturized cell surfaces result in greater power output.

These conclusions are in agreement with conclusions established in the earlier report.

TABLE NUMBERING SYSTEM

Table	Dependent Variable	Cell	Coating Refractive Index
A-1	Power Output	Plain, uncoated	N/A
A-2	Power Output	Texturized, uncoated	N/A
A-3A	Power Output	Plain, coated	2.0
A-3B	Power Output	Texturized, coated	2.0
A-4A	Power Output	Plain, coated	2.2
A-4B	Power Output	Texturized, coated	2.2
A-5A	Power Output	Plain, coated	2.4
A-5B	Power Output	Texturized, coated	2.4
A-6A	Power Output	Plain, coated	2.6
A-6B	Power Output	Texturized, coated	2.6
A-7A	Power Output	Plain, coated	2.8
A-7B	Power Output	Texturized, coated	2.8
A-8A	Power Output	Plain, coated	3.0
A-8B	Power Output	Texturized, coated	3.0
A-9	Module Conversion Efficiency	Plain, uncoated	N/A
A-10	Module Conversion Efficiency	Texturized, uncoated	N/A
A-11A	Module Conversion Efficiency	Plain, coated	2.0
A-11B	Module Conversion Efficiency	Texturized, coated	2.0
A-12A	Module Conversion Efficiency	Plain, coated	2.2
A-12B	Module Conversion Efficiency	Texturized, coated	2.2
A-13A	Module Conversion Efficiency	Plain, coated	2.4
A-13B	Module Conversion Efficiency	Texturized, coated	2.4
A-14A	Module Conversion Efficiency	Plain, coated	2.6
A-14B	Module Conversion Efficiency	Texturized, coated	2.6
A-15A	Module Conversion Efficiency	Plain, coated	2.8
A-15B	Module Conversion Efficiency	Texturized, coated	2.8
A-16A	Module Conversion Efficiency	Plain, coated	3.0
A-16B	Module Conversion Efficiency	Texturized, coated	3.0

TABLE A-1. MODULE POWER OUTPUT (WATTS) AT AM 1.5 PLAIN SILICON

POTTANT INDEX OF REFRACTION N	COVER INDEX OF REFRACTION-N										
	1.0	1.1	1.2	1.3	1.4	1.5	1.6	1.7	1.8	1.9	2.0
1.0	1.17	1.16	1.15	1.14	1.12	1.10	1.08	1.06	1.04	1.02	1.00
1.1	1.23	1.23	1.22	1.21	1.19	1.17	1.15	1.13	1.11	1.09	1.07
1.2	1.28	1.28	1.28	1.27	1.26	1.24	1.22	1.20	1.17	1.15	1.13
1.3	1.32	1.33	1.33	1.32	1.31	1.29	1.27	1.25	1.23	1.21	1.18
1.4	1.36	1.37	1.37	1.37	1.36	1.34	1.32	1.30	1.28	1.26	1.23
1.5	1.38	1.40	1.41	1.40	1.40	1.38	1.37	1.35	1.32	1.30	1.28
1.6	1.40	1.42	1.43	1.43	1.43	1.42	1.40	1.38	1.36	1.34	1.32
1.7	1.42	1.44	1.45	1.46	1.46	1.45	1.43	1.42	1.40	1.37	1.35
1.8	1.42	1.45	1.47	1.48	1.48	1.47	1.46	1.44	1.42	1.40	1.38
1.9	1.43	1.46	1.48	1.49	1.49	1.49	1.48	1.46	1.45	1.43	1.41
2.0	1.43	1.46	1.49	1.50	1.51	1.50	1.49	1.48	1.47	1.45	1.43

TABLE A-2. MODULE POWER OUTPUT (WATTS) AT AM 1.5 TEXTURIZED CELL

POTTANT INDEX OF REFRACTION N	COVER INDEX OF REFRACTION-N										
	1.0	1.1	1.2	1.3	1.4	1.5	1.6	1.7	1.8	1.9	2.0
1.0	1.48	1.47	1.46	1.43	1.41	1.38	1.35	1.32	1.28	1.25	1.22
1.1	1.51	1.51	1.50	1.48	1.46	1.43	1.40	1.37	1.34	1.31	1.27
1.2	1.53	1.54	1.53	1.52	1.50	1.47	1.45	1.42	1.39	1.35	1.32
1.3	1.55	1.56	1.56	1.55	1.53	1.51	1.48	1.45	1.42	1.39	1.36
1.4	1.55	1.57	1.57	1.56	1.55	1.53	1.51	1.48	1.45	1.42	1.39
1.5	1.55	1.57	1.58	1.57	1.56	1.55	1.53	1.50	1.47	1.45	1.42
1.6	1.54	1.56	1.58	1.58	1.57	1.56	1.54	1.52	1.49	1.46	1.44
1.7	1.53	1.55	1.57	1.58	1.57	1.56	1.55	1.53	1.50	1.48	1.45
1.8	1.51	1.54	1.56	1.57	1.57	1.56	1.55	1.53	1.51	1.49	1.46
1.9	1.49	1.53	1.55	1.56	1.57	1.56	1.55	1.53	1.51	1.49	1.47
2.0	1.47	1.51	1.54	1.55	1.56	1.55	1.55	1.53	1.52	1.50	1.47

TABLE A-3A. MODULE POWER OUTPUT (WATTS) AT AM 1.5 AR COATING, N = 2.0

POTTANT INDEX OF REFRACTION N	COVER INDEX OF REFRACTION-N										
	1.0	1.1	1.2	1.3	1.4	1.5	1.6	1.7	1.8	1.9	2.0
1.0	1.65	1.64	1.62	1.59	1.56	1.53	1.49	1.45	1.41	1.37	1.33
1.1	1.66	1.66	1.65	1.62	1.60	1.56	1.53	1.49	1.45	1.42	1.38
1.2	1.66	1.66	1.66	1.64	1.62	1.59	1.56	1.52	1.48	1.45	1.41
1.3	1.64	1.66	1.66	1.64	1.63	1.60	1.57	1.54	1.51	1.47	1.44
1.4	1.62	1.64	1.65	1.64	1.62	1.60	1.58	1.55	1.52	1.48	1.45
1.5	1.60	1.62	1.63	1.63	1.61	1.60	1.57	1.55	1.52	1.49	1.46
1.6	1.57	1.59	1.61	1.61	1.60	1.59	1.57	1.54	1.52	1.49	1.46
1.7	1.53	1.56	1.58	1.58	1.58	1.57	1.55	1.53	1.51	1.48	1.46
1.8	1.50	1.53	1.55	1.56	1.56	1.55	1.54	1.52	1.50	1.48	1.45
1.9	1.46	1.50	1.52	1.53	1.53	1.53	1.52	1.50	1.48	1.46	1.44
2.0	1.43	1.46	1.49	1.50	1.51	1.50	1.49	1.48	1.47	1.45	1.43

TABLE A-3B. MODULE POWER OUTPUT (WATTS) AT AM 1.5 TEXTURIZED WITH AR COATING, N = 2.0

POTTANT INDEX OF REFRACTION N	COVER INDEX OF REFRACTION-N										
	1.0	1.1	1.2	1.3	1.4	1.5	1.6	1.7	1.8	1.9	2.0
1.0	1.65	1.64	1.63	1.60	1.57	1.53	1.49	1.45	1.41	1.37	1.34
1.1	1.65	1.65	1.64	1.62	1.59	1.56	1.52	1.48	1.45	1.41	1.37
1.2	1.64	1.65	1.64	1.63	1.60	1.57	1.54	1.51	1.47	1.44	1.40
1.3	1.63	1.64	1.64	1.63	1.61	1.59	1.56	1.53	1.49	1.46	1.42
1.4	1.61	1.63	1.63	1.63	1.61	1.59	1.57	1.54	1.51	1.47	1.44
1.5	1.59	1.61	1.62	1.62	1.61	1.59	1.57	1.54	1.52	1.49	1.45
1.6	1.57	1.60	1.61	1.61	1.60	1.59	1.57	1.55	1.52	1.49	1.46
1.7	1.55	1.58	1.59	1.60	1.60	1.59	1.57	1.55	1.52	1.50	1.47
1.8	1.52	1.56	1.58	1.59	1.59	1.58	1.56	1.55	1.52	1.50	1.47
1.9	1.50	1.54	1.56	1.57	1.57	1.57	1.56	1.54	1.52	1.50	1.47
2.0	1.47	1.51	1.54	1.55	1.56	1.55	1.55	1.53	1.52	1.50	1.47

TABLE A-4A. MODULE POWER OUTPUT (WATTS) AT AM 1.5 AR COATING, N = 2.2

POTTANT INDEX OF REFRACTION N	COVER INDEX OF REFRACTION-N										
	1.0	1.1	1.2	1.3	1.4	1.5	1.6	1.7	1.8	1.9	2.0
1.0	1.63	1.62	1.60	1.57	1.54	1.51	1.47	1.43	1.39	1.36	1.32
1.1	1.65	1.65	1.64	1.62	1.59	1.56	1.52	1.48	1.45	1.41	1.37
1.2	1.66	1.67	1.66	1.64	1.62	1.59	1.56	1.52	1.49	1.45	1.41
1.3	1.66	1.67	1.67	1.66	1.64	1.61	1.58	1.55	1.52	1.48	1.44
1.4	1.65	1.66	1.67	1.66	1.65	1.62	1.60	1.57	1.54	1.50	1.47
1.5	1.63	1.65	1.66	1.66	1.65	1.63	1.60	1.58	1.55	1.52	1.48
1.6	1.60	1.63	1.65	1.65	1.64	1.62	1.60	1.58	1.55	1.52	1.49
1.7	1.58	1.61	1.63	1.63	1.63	1.62	1.60	1.58	1.55	1.53	1.50
1.8	1.55	1.58	1.60	1.61	1.61	1.60	1.59	1.57	1.55	1.52	1.50
1.9	1.51	1.55	1.58	1.59	1.59	1.58	1.57	1.56	1.54	1.51	1.49
2.0	1.48	1.52	1.55	1.56	1.57	1.57	1.56	1.54	1.53	1.50	1.48

TABLE A-4B. MODULE POWER OUTPUT (WATTS) AT AM 1.5 TEXTURIZED WITH AR COATING, N = 2.2

POTTANT INDEX OF REFRACTION N	COVER INDEX OF REFRACTION-N										
	1.0	1.1	1.2	1.3	1.4	1.5	1.6	1.7	1.8	1.9	2.0
1.0	1.65	1.64	1.62	1.60	1.56	1.53	1.49	1.45	1.41	1.37	1.33
1.1	1.65	1.65	1.64	1.62	1.59	1.56	1.52	1.48	1.45	1.41	1.37
1.2	1.64	1.65	1.64	1.63	1.60	1.57	1.54	1.51	1.47	1.44	1.40
1.3	1.63	1.64	1.64	1.63	1.61	1.59	1.56	1.53	1.49	1.46	1.42
1.4	1.61	1.63	1.64	1.63	1.61	1.59	1.57	1.54	1.51	1.48	1.44
1.5	1.59	1.62	1.63	1.62	1.61	1.59	1.57	1.55	1.52	1.49	1.46
1.6	1.57	1.60	1.61	1.61	1.61	1.59	1.57	1.55	1.52	1.50	1.47
1.7	1.55	1.58	1.60	1.60	1.60	1.59	1.57	1.55	1.53	1.50	1.47
1.8	1.53	1.56	1.58	1.59	1.59	1.58	1.57	1.55	1.53	1.50	1.48
1.9	1.50	1.54	1.56	1.58	1.58	1.57	1.56	1.55	1.53	1.50	1.48
2.0	1.48	1.52	1.55	1.56	1.57	1.56	1.55	1.54	1.52	1.50	1.48

TABLE A-5A. MODULE POWER OUTPUT (WATTS) AT AM 1.5 AR COATING, N = 2.4

POTTANT INDEX OF REFRACTION N	COVER INDEX OF REFRACTION-N										
	1.0	1.1	1.2	1.3	1.4	1.5	1.6	1.7	1.8	1.9	2.0
1.0	1.59	1.58	1.56	1.54	1.51	1.47	1.44	1.40	1.36	1.33	1.29
1.1	1.62	1.62	1.61	1.59	1.56	1.53	1.50	1.46	1.42	1.39	1.35
1.2	1.64	1.65	1.64	1.62	1.60	1.57	1.54	1.51	1.47	1.43	1.40
1.3	1.65	1.66	1.66	1.65	1.63	1.60	1.57	1.54	1.51	1.47	1.44
1.4	1.64	1.66	1.67	1.66	1.64	1.62	1.60	1.57	1.53	1.50	1.47
1.5	1.63	1.66	1.67	1.66	1.65	1.63	1.61	1.58	1.55	1.52	1.49
1.6	1.62	1.65	1.66	1.66	1.65	1.64	1.62	1.59	1.57	1.54	1.50
1.7	1.60	1.63	1.65	1.65	1.65	1.64	1.62	1.60	1.57	1.54	1.51
1.8	1.57	1.61	1.63	1.64	1.64	1.63	1.61	1.60	1.57	1.55	1.52
1.9	1.55	1.58	1.61	1.62	1.62	1.62	1.61	1.59	1.57	1.55	1.52
2.0	1.52	1.56	1.59	1.60	1.61	1.60	1.59	1.58	1.56	1.54	1.52

TABLE A-5B. MODULE POWER OUTPUT (WATTS) AT AM 1.5 TEXTURIZED WITH AR COATING, N = 1.4

POTTANT INDEX OF REFRACTION N	COVER INDEX OF REFRACTION-N										
	1.0	1.1	1.2	1.3	1.4	1.5	1.6	1.7	1.8	1.9	2.0
1.0	1.64	1.64	1.62	1.59	1.56	1.52	1.49	1.45	1.41	1.37	1.33
1.1	1.65	1.65	1.63	1.61	1.58	1.55	1.52	1.48	1.44	1.41	1.37
1.2	1.64	1.65	1.64	1.62	1.60	1.57	1.54	1.51	1.47	1.44	1.40
1.3	1.63	1.64	1.64	1.63	1.61	1.59	1.56	1.53	1.49	1.46	1.42
1.4	1.61	1.63	1.64	1.63	1.61	1.59	1.57	1.54	1.51	1.48	1.44
1.5	1.60	1.62	1.63	1.62	1.61	1.60	1.57	1.55	1.52	1.49	1.46
1.6	1.57	1.60	1.61	1.62	1.61	1.59	1.57	1.55	1.52	1.50	1.47
1.7	1.55	1.58	1.60	1.61	1.60	1.59	1.57	1.55	1.53	1.50	1.47
1.8	1.53	1.56	1.58	1.59	1.59	1.58	1.57	1.55	1.53	1.51	1.48
1.9	1.51	1.54	1.57	1.58	1.58	1.58	1.56	1.55	1.53	1.51	1.48
2.0	1.48	1.52	1.55	1.56	1.57	1.57	1.56	1.54	1.53	1.51	1.48

TABLE A-6A. MODULE POWER OUTPUT (WATTS) AT AM 1.5 AR COATING, N = 2.6

POTTANT INDEX OF REFRACTION N	COVER INDEX OF REFRACTION-N										
	1.0	1.1	1.2	1.3	1.4	1.5	1.6	1.7	1.8	1.9	2.0
1.0	1.53	1.53	1.51	1.49	1.46	1.43	1.39	1.36	1.33	1.29	1.26
1.1	1.58	1.58	1.56	1.54	1.52	1.49	1.46	1.42	1.39	1.35	1.32
1.2	1.60	1.61	1.60	1.59	1.57	1.54	1.51	1.48	1.44	1.41	1.37
1.3	1.62	1.63	1.63	1.62	1.60	1.58	1.55	1.52	1.48	1.45	1.42
1.4	1.63	1.64	1.65	1.64	1.63	1.60	1.58	1.55	1.52	1.49	1.45
1.5	1.62	1.65	1.65	1.65	1.64	1.62	1.60	1.57	1.54	1.51	1.48
1.6	1.61	1.64	1.65	1.66	1.65	1.63	1.61	1.59	1.56	1.53	1.50
1.7	1.60	1.63	1.65	1.65	1.65	1.64	1.62	1.60	1.57	1.55	1.52
1.8	1.58	1.62	1.64	1.65	1.65	1.64	1.62	1.60	1.58	1.55	1.53
1.9	1.56	1.60	1.62	1.63	1.64	1.63	1.62	1.60	1.58	1.56	1.53
2.0	1.53	1.58	1.60	1.62	1.63	1.62	1.61	1.60	1.58	1.56	1.53

TABLE A-6B. MODULE POWER OUTPUT (WATTS) AT AM 1.5 TEXTURIZED WITH AR COATING, N = 2.6

POTTANT INDEX OF REFRACTION N	COVER INDEX OF REFRACTION-N										
	1.0	1.1	1.2	1.3	1.4	1.5	1.6	1.7	1.8	1.9	2.0
1.0	1.63	1.63	1.61	1.58	1.55	1.52	1.48	1.44	1.40	1.36	1.32
1.1	1.64	1.64	1.63	1.61	1.58	1.55	1.51	1.48	1.44	1.40	1.36
1.2	1.64	1.64	1.64	1.62	1.60	1.57	1.54	1.50	1.47	1.43	1.40
1.3	1.63	1.64	1.64	1.63	1.61	1.58	1.55	1.52	1.49	1.46	1.42
1.4	1.61	1.63	1.63	1.63	1.61	1.59	1.57	1.54	1.51	1.47	1.44
1.5	1.59	1.62	1.63	1.62	1.61	1.59	1.57	1.55	1.52	1.49	1.46
1.6	1.57	1.60	1.61	1.62	1.61	1.59	1.57	1.55	1.52	1.50	1.47
1.7	1.55	1.58	1.60	1.61	1.60	1.59	1.57	1.55	1.53	1.50	1.47
1.8	1.53	1.56	1.58	1.59	1.59	1.58	1.57	1.55	1.53	1.51	1.48
1.9	1.51	1.54	1.57	1.58	1.58	1.58	1.56	1.55	1.53	1.51	1.48
2.0	1.48	1.52	1.55	1.56	1.57	1.57	1.56	1.54	1.53	1.51	1.48

TABLE A-7A. MODULE POWER OUTPUT (WATTS) AT AM 1.5 AR COATING, N = 2.8

POTTANT INDEX OF REFRACTION N	COVER INDEX OF REFRACTION-N										
	1.0	1.1	1.2	1.3	1.4	1.5	1.6	1.7	1.8	1.9	2.0
1.0	1.47	1.47	1.45	1.43	1.40	1.37	1.34	1.31	1.28	1.25	1.22
1.1	1.52	1.52	1.51	1.49	1.47	1.44	1.41	1.38	1.35	1.31	1.28
1.2	1.56	1.56	1.56	1.54	1.52	1.50	1.47	1.44	1.40	1.37	1.34
1.3	1.58	1.59	1.59	1.58	1.56	1.54	1.51	1.48	1.45	1.42	1.39
1.4	1.59	1.61	1.61	1.61	1.59	1.57	1.55	1.52	1.49	1.46	1.43
1.5	1.60	1.62	1.63	1.63	1.61	1.60	1.57	1.55	1.52	1.49	1.46
1.6	1.59	1.62	1.63	1.64	1.63	1.61	1.59	1.57	1.54	1.51	1.48
1.7	1.59	1.62	1.63	1.64	1.64	1.62	1.61	1.59	1.56	1.53	1.50
1.8	1.57	1.61	1.63	1.64	1.64	1.63	1.61	1.60	1.57	1.55	1.52
1.9	1.56	1.59	1.62	1.63	1.63	1.63	1.62	1.60	1.58	1.56	1.53
2.0	1.54	1.58	1.61	1.62	1.63	1.62	1.62	1.60	1.58	1.56	1.54

TABLE A-7B. MODULE POWER OUTPUT (WATTS) AT AM 1.5 TEXTURIZED WITH AR COATING, N = 2.8

POTTANT INDEX OF REFRACTION N	COVER INDEX OF REFRACTION-N										
	1.0	1.1	1.2	1.3	1.4	1.5	1.6	1.7	1.8	1.9	2.0
1.0	1.62	1.61	1.59	1.57	1.54	1.50	1.46	1.43	1.39	1.35	1.31
1.1	1.63	1.63	1.62	1.60	1.57	1.54	1.50	1.47	1.43	1.39	1.36
1.2	1.63	1.64	1.63	1.61	1.59	1.56	1.53	1.50	1.46	1.43	1.39
1.3	1.62	1.63	1.63	1.62	1.60	1.58	1.55	1.52	1.49	1.45	1.42
1.4	1.61	1.63	1.63	1.62	1.61	1.59	1.56	1.53	1.50	1.47	1.44
1.5	1.59	1.61	1.62	1.62	1.61	1.59	1.57	1.54	1.52	1.49	1.45
1.6	1.57	1.60	1.61	1.61	1.61	1.59	1.57	1.55	1.52	1.50	1.47
1.7	1.55	1.58	1.60	1.60	1.60	1.59	1.57	1.55	1.53	1.50	1.47
1.8	1.53	1.56	1.58	1.59	1.59	1.58	1.57	1.55	1.53	1.51	1.48
1.9	1.51	1.54	1.57	1.58	1.58	1.58	1.56	1.55	1.53	1.51	1.48
2.0	1.48	1.52	1.55	1.56	1.57	1.57	1.56	1.54	1.53	1.51	1.48

TABLE A-8A. MODULE POWER OUTPUT (WATTS) AT AM 1.5 AR COATING, N = 3.0

POTTANT INDEX OF REFRACTION N	COVER INDEX OF REFRACTION-N										
	1.0	1.1	1.2	1.3	1.4	1.5	1.6	1.7	1.8	1.9	2.0
1.0	1.41	1.40	1.39	1.37	1.34	1.32	1.29	1.26	1.23	1.20	1.17
1.1	1.46	1.46	1.45	1.43	1.41	1.39	1.36	1.33	1.30	1.27	1.24
1.2	1.50	1.51	1.50	1.49	1.47	1.44	1.42	1.39	1.36	1.33	1.30
1.3	1.53	1.54	1.54	1.53	1.51	1.49	1.47	1.44	1.41	1.38	1.35
1.4	1.55	1.57	1.57	1.56	1.55	1.53	1.51	1.48	1.45	1.42	1.39
1.5	1.56	1.58	1.59	1.59	1.58	1.56	1.54	1.51	1.49	1.46	1.43
1.6	1.56	1.59	1.60	1.60	1.60	1.58	1.56	1.54	1.52	1.49	1.46
1.7	1.56	1.59	1.61	1.61	1.61	1.60	1.58	1.56	1.54	1.51	1.48
1.8	1.55	1.59	1.61	1.62	1.62	1.61	1.59	1.58	1.55	1.53	1.50
1.9	1.54	1.58	1.60	1.62	1.62	1.61	1.60	1.59	1.56	1.54	1.52
2.0	1.53	1.57	1.60	1.61	1.62	1.61	1.60	1.59	1.57	1.55	1.53

TABLE A-8B. MODULE POWER OUTPUT (WATTS) AT AM 1.5 TEXTURIZED WITH AR COATING, N = 3.0

POTTANT INDEX OF REFRACTION N	COVER INDEX OF REFRACTION-N										
	1.0	1.1	1.2	1.3	1.4	1.5	1.6	1.7	1.8	1.9	2.0
1.0	1.60	1.59	1.57	1.55	1.52	1.48	1.45	1.41	1.37	1.34	1.30
1.1	1.61	1.61	1.60	1.58	1.55	1.52	1.49	1.45	1.42	1.38	1.35
1.2	1.62	1.62	1.62	1.60	1.58	1.55	1.52	1.49	1.45	1.42	1.38
1.3	1.61	1.63	1.62	1.61	1.59	1.57	1.54	1.51	1.48	1.45	1.41
1.4	1.60	1.62	1.62	1.62	1.60	1.58	1.56	1.53	1.50	1.47	1.43
1.5	1.59	1.61	1.62	1.62	1.61	1.59	1.57	1.54	1.51	1.48	1.45
1.6	1.57	1.60	1.61	1.61	1.60	1.59	1.57	1.55	1.52	1.49	1.46
1.7	1.55	1.58	1.60	1.60	1.60	1.59	1.57	1.55	1.53	1.50	1.47
1.8	1.53	1.56	1.58	1.59	1.59	1.58	1.57	1.55	1.53	1.50	1.48
1.9	1.51	1.54	1.57	1.58	1.58	1.58	1.56	1.55	1.53	1.51	1.48
2.0	1.48	1.52	1.55	1.56	1.57	1.57	1.56	1.54	1.53	1.51	1.48

TABLE A-9. MODULE POWER CONVERSION EFFICIENCY AT AM 1.5
PLAIN SILICON
ELECTRICAL POWER OUT/INCIDENT POWER

COVER
INDEX OF REFRACTION-N

POTTANT INDEX OF REFRACTION N	1.0	1.1	1.2	1.3	1.4	1.5	1.6	1.7	1.8	1.9	2.0
1.0	0.10	0.10	0.10	0.09	0.09	0.09	0.09	0.09	0.09	0.08	0.08
1.1	0.10	0.10	0.10	0.10	0.10	0.10	0.10	0.09	0.09	0.09	0.09
1.2	0.11	0.11	0.11	0.10	0.10	0.10	0.10	0.10	0.10	0.10	0.09
1.3	0.11	0.11	0.11	0.11	0.11	0.11	0.11	0.10	0.10	0.10	0.10
1.4	0.11	0.11	0.11	0.11	0.11	0.11	0.11	0.11	0.11	0.10	0.10
1.5	0.11	0.12	0.12	0.12	0.12	0.11	0.11	0.11	0.11	0.11	0.11
1.6	0.12	0.12	0.12	0.12	0.12	0.12	0.12	0.11	0.11	0.11	0.11
1.7	0.12	0.12	0.12	0.12	0.12	0.12	0.12	0.12	0.12	0.11	0.11
1.8	0.12	0.12	0.12	0.12	0.12	0.12	0.12	0.12	0.12	0.12	0.11
1.9	0.12	0.12	0.12	0.12	0.12	0.12	0.12	0.12	0.12	0.12	0.12
2.0	0.12	0.12	0.12	0.12	0.12	0.12	0.12	0.12	0.12	0.12	0.12

TABLE A-10. MODULE POWER CONVERSION EFFICIENCY AT AM 1.5
TEXTURIZED CELL
ELECTRICAL POWER OUT/INCIDENT POWER

COVER
INDEX OF REFRACTION-N

POTTANT INDEX OF EFRACTION N	1.0	1.1	1.2	1.3	1.4	1.5	1.6	1.7	1.8	1.9	2.0
1.0	0.12	0.12	0.12	0.12	0.12	0.11	0.11	0.11	0.11	0.10	0.10
1.1	0.12	0.12	0.12	0.12	0.12	0.12	0.12	0.11	0.11	0.11	0.11
1.2	0.13	0.13	0.13	0.13	0.12	0.12	0.12	0.12	0.11	0.11	0.11
1.3	0.13	0.13	0.13	0.13	0.13	0.12	0.12	0.12	0.12	0.12	0.11
1.4	0.13	0.13	0.13	0.13	0.13	0.13	0.12	0.12	0.12	0.12	0.11
1.5	0.13	0.13	0.13	0.13	0.13	0.13	0.13	0.12	0.12	0.12	0.12
1.6	0.13	0.13	0.13	0.13	0.13	0.13	0.13	0.13	0.12	0.12	0.12
1.7	0.13	0.13	0.13	0.13	0.13	0.13	0.13	0.13	0.12	0.12	0.12
1.8	0.12	0.13	0.13	0.13	0.13	0.13	0.13	0.13	0.12	0.12	0.12
1.9	0.12	0.13	0.13	0.13	0.13	0.13	0.13	0.13	0.13	0.12	0.12
2.0	0.12	0.13	0.13	0.13	0.13	0.13	0.13	0.13	0.13	0.12	0.12

TABLE A-11A. MODULE POWER CONVERSION EFFICIENCY AT AM 1.5
AR COATING, N = 2.0
ELECTRICAL POWER OUT/INCIDENT POWER

		COVER INDEX OF REFRACTION-N										
		1.0	1.1	1.2	1.3	1.4	1.5	1.6	1.7	1.8	1.9	2.0
POTTANT INDEX OF REFRACTION N	1.0	0.14	0.14	0.13	0.13	0.13	0.13	0.12	0.12	0.12	0.11	0.11
	1.1	0.14	0.14	0.14	0.13	0.13	0.13	0.13	0.12	0.12	0.12	0.11
	1.2	0.14	0.14	0.14	0.14	0.13	0.13	0.13	0.13	0.12	0.12	0.12
	1.3	0.14	0.14	0.14	0.14	0.13	0.13	0.13	0.13	0.12	0.12	0.12
	1.4	0.13	0.14	0.14	0.14	0.13	0.13	0.13	0.13	0.13	0.12	0.12
	1.5	0.13	0.13	0.13	0.13	0.13	0.13	0.13	0.13	0.13	0.12	0.12
	1.6	0.13	0.13	0.13	0.13	0.13	0.13	0.13	0.13	0.13	0.12	0.12
	1.7	0.13	0.13	0.13	0.13	0.13	0.13	0.13	0.13	0.12	0.12	0.12
	1.8	0.12	0.13	0.13	0.13	0.13	0.13	0.13	0.13	0.12	0.12	0.12
	1.9	0.12	0.12	0.13	0.13	0.13	0.13	0.13	0.12	0.12	0.12	0.12
	2.0	0.12	0.12	0.12	0.12	0.12	0.12	0.12	0.12	0.12	0.12	0.12

TABLE A-11B. MODULE POWER CONVERSION EFFICIENCY AT AM 1.5
TEXTURIZED WITH AR COATING, N = 2.0
ELECTRICAL POWER OUT/INCIDENT POWER

		COVER INDEX REFRACTION-N										
		1.0	1.1	1.2	1.3	1.4	1.5	1.6	1.7	1.8	1.9	2.0
POTTANT INDEX OF REFRACTION N	1.0	0.14	0.14	0.13	0.13	0.13	0.13	0.12	0.12	0.12	0.11	0.11
	1.1	0.14	0.14	0.14	0.13	0.13	0.13	0.13	0.12	0.12	0.12	0.11
	1.2	0.14	0.14	0.14	0.13	0.13	0.13	0.13	0.12	0.12	0.12	0.12
	1.3	0.13	0.14	0.14	0.13	0.13	0.13	0.13	0.13	0.12	0.12	0.12
	1.4	0.13	0.13	0.14	0.13	0.13	0.13	0.13	0.13	0.12	0.12	0.12
	1.5	0.13	0.13	0.13	0.13	0.13	0.13	0.13	0.13	0.13	0.12	0.12
	1.6	0.13	0.13	0.13	0.13	0.13	0.13	0.13	0.13	0.13	0.12	0.12
	1.7	0.13	0.13	0.13	0.13	0.13	0.13	0.13	0.13	0.13	0.12	0.12
	1.8	0.13	0.13	0.13	0.13	0.13	0.13	0.13	0.13	0.13	0.12	0.12
	1.9	0.12	0.13	0.13	0.13	0.13	0.13	0.13	0.13	0.13	0.12	0.12
	2.0	0.12	0.13	0.13	0.13	0.13	0.13	0.13	0.13	0.13	0.12	0.12

TABLE A-12A. MODULE POWER CONVERSION EFFICIENCY AT AM 1.5
AR COATING, N = 2.2
ELECTRICAL POWER OUT/INCIDENT POWER

POTTANT INDEX OF REFRACTION N	COVER INDEX OF REFRACTION-N										
	1.0	1.1	1.2	1.3	1.4	1.5	1.6	1.7	1.8	1.9	2.0
1.0	0.13	0.13	0.13	0.13	0.13	0.12	0.12	0.12	0.12	0.11	0.11
1.1	0.14	0.14	0.14	0.13	0.13	0.13	0.13	0.12	0.12	0.12	0.11
1.2	0.14	0.14	0.14	0.14	0.13	0.13	0.13	0.13	0.12	0.12	0.12
1.3	0.14	0.14	0.14	0.14	0.14	0.13	0.13	0.13	0.13	0.12	0.12
1.4	0.14	0.14	0.14	0.14	0.14	0.13	0.13	0.13	0.13	0.12	0.12
1.5	0.13	0.14	0.14	0.14	0.14	0.13	0.13	0.13	0.13	0.13	0.12
1.6	0.13	0.13	0.14	0.14	0.14	0.13	0.13	0.13	0.13	0.13	0.12
1.7	0.13	0.13	0.13	0.13	0.13	0.13	0.13	0.13	0.13	0.13	0.12
1.8	0.13	0.13	0.13	0.13	0.13	0.13	0.13	0.13	0.13	0.13	0.12
1.9	0.13	0.13	0.13	0.13	0.13	0.13	0.13	0.13	0.13	0.13	0.12
2.0	0.12	0.13	0.13	0.13	0.13	0.13	0.13	0.13	0.13	0.12	0.12

TABLE A-12B. MODULE POWER CONVERSION EFFICIENCY AT AM 1.5
TEXTURIZED WITH AR COATING, N = 2.2
ELECTRICAL POWER OUT/INCIDENT POWER

POTTANT INDEX OF REFRACTION N	COVER INDEX OF REFRACTION-N										
	1.0	1.1	1.2	1.3	1.4	1.5	1.6	1.7	1.8	1.9	2.0
1.0	0.14	0.14	0.13	0.13	0.13	0.13	0.12	0.12	0.12	0.11	0.11
1.1	0.14	0.14	0.14	0.13	0.13	0.13	0.13	0.12	0.12	0.12	0.11
1.2	0.14	0.14	0.14	0.13	0.13	0.13	0.13	0.12	0.12	0.12	0.12
1.3	0.13	0.14	0.14	0.13	0.13	0.13	0.13	0.13	0.12	0.12	0.12
1.4	0.13	0.13	0.14	0.13	0.13	0.13	0.13	0.13	0.12	0.12	0.12
1.5	0.13	0.13	0.13	0.13	0.13	0.13	0.13	0.13	0.13	0.12	0.12
1.6	0.13	0.13	0.13	0.13	0.13	0.13	0.13	0.13	0.13	0.12	0.12
1.7	0.13	0.13	0.13	0.13	0.13	0.13	0.13	0.13	0.13	0.12	0.12
1.8	0.13	0.13	0.13	0.13	0.13	0.13	0.13	0.13	0.13	0.12	0.12
1.9	0.12	0.13	0.13	0.13	0.13	0.13	0.13	0.13	0.13	0.12	0.12
2.0	0.12	0.13	0.13	0.13	0.13	0.13	0.13	0.13	0.13	0.12	0.12

TABLE A-13A. MODULE POWER CONVERSION EFFICIENCY AT AM 1.5
AR COATING, N = 2.4
ELECTRICAL POWER OUT/INCIDENT POWER

POTTANT INDEX OF REFRACTION N	COVER INDEX OR REFRACTION-N										
	1.0	1.1	1.2	1.3	1.4	1.5	1.6	1.7	1.8	1.9	2.0
1.0	0.13	0.13	0.13	0.13	0.12	0.12	0.12	0.12	0.11	0.11	0.11
1.1	0.13	0.13	0.13	0.13	0.13	0.13	0.12	0.12	0.12	0.11	0.11
1.2	0.14	0.14	0.14	0.13	0.13	0.13	0.13	0.12	0.12	0.12	0.12
1.3	0.14	0.14	0.14	0.14	0.13	0.13	0.13	0.13	0.12	0.12	0.12
1.4	0.14	0.14	0.14	0.14	0.14	0.13	0.13	0.13	0.13	0.12	0.12
1.5	0.14	0.14	0.14	0.14	0.14	0.14	0.13	0.13	0.13	0.13	0.12
1.6	0.13	0.14	0.14	0.14	0.14	0.14	0.13	0.13	0.13	0.13	0.12
1.7	0.13	0.13	0.14	0.14	0.14	0.14	0.13	0.13	0.13	0.13	0.13
1.8	0.13	0.13	0.13	0.14	0.14	0.13	0.13	0.13	0.13	0.13	0.13
1.9	0.13	0.13	0.13	0.13	0.13	0.13	0.13	0.13	0.13	0.13	0.13
2.0	0.13	0.13	0.13	0.13	0.13	0.13	0.13	0.13	0.13	0.13	0.13

TABLE A-13B. MODULE POWER CONVERSION EFFICIENCY AT AM 1.5
TEXTURIZED WITH AR COATING, N = 2.4
ELECTRICAL POWER OUT/INCIDENT POWER

POTTANT INDEX OF REFRACTION N	COVER INDEX OR REFRACTION-N										
	1.0	1.1	1.2	1.3	1.4	1.5	1.6	1.7	1.8	1.9	2.0
1.0	0.14	0.14	0.13	0.13	0.13	0.13	0.12	0.12	0.12	0.11	0.11
1.1	0.14	0.14	0.14	0.13	0.13	0.13	0.13	0.12	0.12	0.12	0.11
1.2	0.14	0.14	0.14	0.13	0.13	0.13	0.13	0.12	0.12	0.12	0.12
1.3	0.13	0.14	0.14	0.13	0.13	0.13	0.13	0.13	0.12	0.12	0.12
1.4	0.13	0.13	0.14	0.13	0.13	0.13	0.13	0.13	0.12	0.12	0.12
1.5	0.13	0.13	0.13	0.13	0.13	0.13	0.13	0.13	0.13	0.12	0.12
1.6	0.13	0.13	0.13	0.13	0.13	0.13	0.13	0.13	0.13	0.12	0.12
1.7	0.13	0.13	0.13	0.13	0.13	0.13	0.13	0.13	0.13	0.12	0.12
1.8	0.13	0.13	0.13	0.13	0.13	0.13	0.13	0.13	0.13	0.12	0.12
1.9	0.12	0.13	0.13	0.13	0.13	0.13	0.13	0.13	0.13	0.12	0.12
2.0	0.12	0.13	0.13	0.13	0.13	0.13	0.13	0.13	0.13	0.12	0.12

TABLE A-14A. MODULE POWER CONVERSION EFFICIENCY AT AM 1.5
AR COATING, N= 2.6
ELECTRICAL POWER OUT/INCIDENT POWER

POTTANT INDEX OF REFRACTION N	COVER INDEX OF REFRACTION-N										
	1.0	1.1	1.2	1.3	1.4	1.5	1.6	1.7	1.8	1.9	2.0
1.0	0.13	0.13	0.12	0.12	0.12	0.12	0.12	0.11	0.11	0.11	0.10
1.1	0.13	0.13	0.13	0.13	0.13	0.12	0.12	0.12	0.11	0.11	0.11
1.2	0.13	0.13	0.13	0.13	0.13	0.13	0.12	0.12	0.12	0.12	0.11
1.3	0.13	0.13	0.13	0.13	0.13	0.13	0.13	0.13	0.12	0.12	0.12
1.4	0.13	0.14	0.14	0.14	0.13	0.13	0.13	0.13	0.13	0.12	0.12
1.5	0.13	0.14	0.14	0.14	0.14	0.13	0.13	0.13	0.13	0.13	0.12
1.6	0.13	0.14	0.14	0.14	0.14	0.14	0.13	0.13	0.13	0.13	0.12
1.7	0.13	0.13	0.14	0.14	0.14	0.14	0.13	0.13	0.13	0.13	0.13
1.8	0.13	0.13	0.14	0.14	0.14	0.14	0.13	0.13	0.13	0.13	0.13
1.9	0.13	0.13	0.13	0.14	0.14	0.13	0.13	0.13	0.13	0.13	0.13
2.0	0.13	0.13	0.13	0.13	0.13	0.13	0.13	0.13	0.13	0.13	0.13

TABLE A-14B. MODULE POWER CONVERSION EFFICIENCY AT AM 1.5
TEXTURIZED WITH AR COATING, N = 2.6
ELECTRICAL POWER OUT/INCIDENT POWER

POTTANT INDEX OF REFRACTION N	COVER INDEX OF REFRACTION-N										
	1.0	1.1	1.2	1.3	1.4	1.5	1.6	1.7	1.8	1.9	2.0
1.0	0.14	0.13	0.13	0.13	0.13	0.13	0.12	0.12	0.12	0.11	0.11
1.1	0.14	0.14	0.13	0.13	0.13	0.13	0.13	0.12	0.12	0.12	0.11
1.2	0.14	0.14	0.14	0.13	0.13	0.13	0.13	0.12	0.12	0.12	0.12
1.3	0.13	0.14	0.14	0.13	0.13	0.13	0.13	0.13	0.12	0.12	0.12
1.4	0.13	0.13	0.14	0.13	0.13	0.13	0.13	0.13	0.12	0.12	0.12
1.5	0.13	0.13	0.13	0.13	0.13	0.13	0.13	0.13	0.13	0.12	0.12
1.6	0.13	0.13	0.13	0.13	0.13	0.13	0.13	0.13	0.13	0.12	0.12
1.7	0.13	0.13	0.13	0.13	0.13	0.13	0.13	0.13	0.13	0.12	0.12
1.8	0.13	0.13	0.13	0.13	0.13	0.13	0.13	0.13	0.13	0.12	0.12
1.9	0.12	0.13	0.13	0.13	0.13	0.13	0.13	0.13	0.13	0.12	0.12
2.0	0.12	0.13	0.13	0.13	0.13	0.13	0.13	0.13	0.13	0.12	0.12

TABLE A-15A. MODULE POWER CONVERSION EFFICIENCY AT AM 1.5
AR COATING, N = 2.8
ELECTRICAL POWER OUT/INCIDENT POWER

COVER
INDEX OF REFRACTION-N

POTTANT INDEX OF REFRACTION N	1.0	1.1	1.2	1.3	1.4	1.5	1.6	1.7	1.8	1.9	2.0
1.0	0.12	0.12	0.12	0.12	0.12	0.11	0.11	0.11	0.11	0.10	0.10
1.1	0.13	0.13	0.12	0.12	0.12	0.12	0.12	0.11	0.11	0.11	0.11
1.2	0.13	0.13	0.13	0.13	0.13	0.12	0.12	0.12	0.12	0.11	0.11
1.3	0.13	0.13	0.13	0.13	0.13	0.13	0.12	0.12	0.12	0.12	0.11
1.4	0.13	0.13	0.13	0.13	0.13	0.13	0.13	0.13	0.12	0.12	0.12
1.5	0.13	0.13	0.13	0.13	0.13	0.13	0.13	0.13	0.13	0.12	0.12
1.6	0.13	0.13	0.14	0.14	0.13	0.13	0.13	0.13	0.13	0.13	0.12
1.7	0.13	0.13	0.14	0.14	0.14	0.13	0.13	0.13	0.13	0.13	0.12
1.8	0.13	0.13	0.13	0.14	0.14	0.13	0.13	0.13	0.13	0.13	0.13
1.9	0.13	0.13	0.13	0.13	0.14	0.13	0.13	0.13	0.13	0.13	0.13
2.0	0.13	0.13	0.13	0.13	0.13	0.13	0.13	0.13	0.13	0.13	0.13

TABLE A-15B. MODULE POWER CONVERSION EFFICIENCY AT AM 1.5
TEXTURIZED WITH AR COATING, N = 2.8
ELECTRICAL POWER OUT/INCIDENT POWER

COVER
INDEX OR REFRACTION-N

POTTANT INDEX OF REFRACTION N	1.0	1.1	1.2	1.3	1.4	1.5	1.6	1.7	1.8	1.9	2.0
1.0	0.13	0.13	0.13	0.13	0.13	0.12	0.12	0.12	0.11	0.11	0.11
1.1	0.13	0.13	0.13	0.13	0.13	0.13	0.12	0.12	0.12	0.12	0.11
1.2	0.13	0.14	0.13	0.13	0.13	0.13	0.13	0.12	0.12	0.12	0.12
1.3	0.13	0.14	0.14	0.13	0.13	0.13	0.13	0.13	0.12	0.12	0.12
1.4	0.13	0.13	0.13	0.13	0.13	0.13	0.13	0.13	0.12	0.12	0.12
1.5	0.13	0.13	0.13	0.13	0.13	0.13	0.13	0.13	0.13	0.12	0.12
1.6	0.13	0.13	0.13	0.13	0.13	0.13	0.13	0.13	0.13	0.12	0.12
1.7	0.13	0.13	0.13	0.13	0.13	0.13	0.13	0.13	0.13	0.12	0.12
1.8	0.13	0.13	0.13	0.13	0.13	0.13	0.13	0.13	0.13	0.12	0.12
1.9	0.12	0.13	0.13	0.13	0.13	0.13	0.13	0.13	0.13	0.12	0.12
2.0	0.12	0.13	0.13	0.13	0.13	0.13	0.13	0.13	0.13	0.12	0.12

TABLE A-16A. MODULE POWER CONVERSION EFFICIENCY AT AM 1.5
AR COATING, N = 3.0
ELECTRICAL POWER OUT/INCIDENT POWER

POTTANT INDEX OF EFRACTION N	COVER INDEX OF REFRACTION-N										
	1.0	1.1	1.2	1.3	1.4	1.5	1.6	1.7	1.8	1.9	2.0
1.0	0.12	0.12	0.11	0.11	0.11	0.11	0.11	0.10	0.10	0.10	0.10
1.1	0.12	0.12	0.12	0.12	0.12	0.11	0.11	0.11	0.11	0.10	0.10
1.2	0.12	0.12	0.12	0.12	0.12	0.12	0.12	0.11	0.11	0.11	0.11
1.3	0.13	0.13	0.13	0.13	0.13	0.12	0.12	0.12	0.12	0.11	0.11
1.4	0.13	0.13	0.13	0.13	0.13	0.13	0.12	0.12	0.12	0.12	0.12
1.5	0.13	0.13	0.13	0.13	0.13	0.13	0.13	0.13	0.12	0.12	0.12
1.6	0.13	0.13	0.13	0.13	0.13	0.13	0.13	0.13	0.13	0.12	0.12
1.7	0.13	0.13	0.13	0.13	0.13	0.13	0.13	0.13	0.13	0.12	0.12
1.8	0.13	0.13	0.13	0.13	0.13	0.13	0.13	0.13	0.13	0.13	0.12
1.9	0.13	0.13	0.13	0.13	0.13	0.13	0.13	0.13	0.13	0.13	0.13
2.0	0.13	0.13	0.13	0.13	0.13	0.13	0.13	0.13	0.13	0.13	0.13

TABLE A-16B. MODULE POWER CONVERSION EFFICIENCY AT AM 1.5
TEXTURIZED WITH AR COATING, N = 3.0
ELECTRICAL POWER OUT/INCIDENT POWER

POTTANT INDEX OF EFRACTION N	COVER INDEX OF REFRACTION-N										
	1.0	1.1	1.2	1.3	1.4	1.5	1.6	1.7	1.8	1.9	2.0
1.0	0.13	0.13	0.13	0.13	0.13	0.12	0.12	0.12	0.11	0.11	0.11
1.1	0.13	0.13	0.13	0.13	0.13	0.13	0.12	0.12	0.12	0.11	0.11
1.2	0.13	0.13	0.13	0.13	0.13	0.13	0.13	0.12	0.12	0.12	0.11
1.3	0.13	0.13	0.13	0.13	0.13	0.13	0.13	0.12	0.12	0.12	0.12
1.4	0.13	0.13	0.13	0.13	0.13	0.13	0.13	0.13	0.12	0.12	0.12
1.5	0.13	0.13	0.13	0.13	0.13	0.13	0.13	0.13	0.13	0.12	0.12
1.6	0.13	0.13	0.13	0.13	0.13	0.13	0.13	0.13	0.13	0.12	0.12
1.7	0.13	0.13	0.13	0.13	0.13	0.13	0.13	0.13	0.13	0.12	0.12
1.8	0.13	0.13	0.13	0.13	0.13	0.13	0.13	0.13	0.13	0.12	0.12
1.9	0.12	0.13	0.13	0.13	0.13	0.13	0.13	0.13	0.13	0.12	0.12
2.0	0.12	0.13	0.13	0.13	0.13	0.13	0.13	0.13	0.13	0.12	0.12